ATTRIBUTION ANALYSIS OF CLOUD FEEDBACK

A Dissertation

by

CHEN ZHOU

Submitted to the Office of Graduate and Professional Studies of
Texas A&M University
in partial fulfillment of the requirements for the degree of

DOCTOR OF PHILOSOPHY

Chair of Committee,	Andrew E. Dessler
Co-Chair of Committee,	Ping Yang
Committee Members,	Gerald R. North
	Anthony M. Filippi
Head of Department,	Ping Yang

August 2014

Major Subject: Atmospheric Sciences

ABSTRACT

Uncertainty on cloud feedback is the primary contributor to the large spread of equilibrium climate sensitivity (ECS) in climate models. In this study, we compare the short-term cloud feedback in climate models with observations, and evaluate the magnitude of long-term cloud feedback predicted by models.

Observations suggest that there are more low clouds in the planetary boundary layer in response to inter-annual surface warming, contributing a strong negative cloud feedback. The overall cloud optical depth decreases, contributing a positive cloud feedback. The overall cloud height in the free atmosphere increases, contributing a positive feedback. The total short-term cloud feedback in response to global surface warming is likely positive.

Climate models generally show a positive cloud feedback in response to surface temperature trend and variability. The spatial pattern of short-term and long-term cloud response is different. However, the vertical profiles of tropical cloud responses to tropical surface temperature trend and variability are the same.

Uncertainty on low cloud amount is the primary source of the large spread in model predicted cloud feedback. Observations suggest that the tropical low cloud fraction increases in response to tropical surface temperature variability, but most climate models show a negative response. The disagreement between models and observations is induced by the poor estimated inversion strength (EIS)-low cloud fraction relationship in climate models. The observed positive short-term tropical low cloud fraction response results

from EIS increase, and changes in large-scale dynamics have little impact on the short-term low cloud response.

Most climate models suggest that tropical EIS will increase under long-term global warming. If the EIS-low cloud fraction relationship holds under global warming, it is likely that the tropical low cloud fraction change is non-negative. Climate models without significant negative low cloud fraction change suggest that the cloud feedback is 0-0.5 $W/m^2/°C$, and the corresponding ECS is 1.5-3.5 °C.

ACKNOWLEDGEMENTS

I would like to express my appreciation to my advisors, Dr. Andrew E. Dessler and Dr. Ping Yang, for their guidance and support. I learnt a lot during my Ph. D. study, and most of them are from my advisors. I would also like to offer my special thanks to my committee members, Dr. Gerald R. North and Dr. Anthony M. Filippi, who helped a lot during my Ph. D. study, and provide me valuable suggestions. I also appreciate the suggestions from Dr. S. A. Klein and Dr. M. D. Zelinka, which are helpful to my research. I thank all my group mates, who helped and discussed with me during my Ph. D. study, and thank my families and friends for their persistent support.

The work was supported by NASA CloudSat/CALIPSO grant NNX10AM27G, NESSF grant NNX12AN57H, and NSF grant AGS-1012665.

NOMENCLATURE

CALIPSO	Cloud-Aerosol Lidar and Infrared Pathfinder Satellite Observation
CERES	Clouds and the Earth's Radiant Energy System
CMIP5	Coupled Model Intercomparison Project phase 5
CRE	Cloud Radiative Effect
ECS	Equilibrium Climate Sensitivity
EIS	Estimated Inversion Strength
ERA-interim	European Centre for Medium-Range Weather Forecasts Interim Reanalysis
ENSO	El Nino-Southern Oscillation
GCM	General Circulation Model
GISTEMP	GISS surface Temperature dataset
ISCCP	International Satellite Cloud Climatology Project
TOA	Top Of Atmosphere
LW	Longwave
MERRA	Modern-Era Retrospective Analysis for Research and Applications
MODIS	Moderate Resolution Imaging Spectroradiometer
MSF	Meridional Mass Stream Function
NH	Northern Hemisphere
PBL	Planetary Boundary Layer
RCP6	Representative Concentration Pathways 6.0
SW	Shortwave

SH	Southern Hemisphere
TTL	Tropical Tropopause Layer

TABLE OF CONTENTS

Page

LIST OF FIGURES

Page

Page

LIST OF TABLES

Page

1. INTRODUCTION

1.1 Global warming and climate sensitivity

Climate change is one of the most important topics in atmospheric sciences. Anthropogenic activities are continuing to change the atmospheric concentrations of greenhouse gases, aerosols, and land surface properties, resulting in a continuing rise in the average temperature of the earth's climate system (Cubasch et al. 2013). The continuing warming of the earth's climate system is referred to as "global warming" by the public.

Global warming has significant impact to the earth's physical systems, biological systems and human systems (Rosenzweig et al. 2007). Future humans may suffer great losses from more extreme events, rising sea levels, and increasing regional vulnerabilities (Schneider et al. 2007). The impact of global warming is decided by the magnitude of future climate changes, and it is important to predict the magnitude of these changes.

The magnitude of global warming is decided by the magnitude of climate radiative forcing and climate sensitivity. The change of equilibrium mean surface temperature can be calculated with

$$\Delta T_s = CS \bullet F \,, \tag{1.1}$$

where F is the climate radiative forcing, defined as an externally imposed perturbation in the radiative energy budget of the Earth's climate system (Houghton et al. 2001); CS is the climate sensitivity, defined as the equilibrium surface temperature change in

response to unit climate radiative forcing. The equilibrium climate sensitivity (ECS) often refers to the global annual mean surface temperature change experienced by the climate system after it has attained a new equilibrium in response to a doubling of atmospheric CO_2 concentration, and the transient climate sensitivity is defined as the global annual mean surface air temperature change over a twenty-year period centered at the time of CO_2 doubling in a 1% per year compound CO_2 increase scenario (Randall et al. 2007).

Unfortunately, there are large uncertainties on both the climate radiative forcing and the climate sensitivity, thus the predicted magnitude of future global warming has large spread among climate change scenarios and among models (Collins et al. 2013).

The equilibrium climate sensitivity in climate models spreads from 1.5K to 4.5K (Sherwood et al. 2014), implying that the global warming magnitude predicted by one climate model could be 2 times larger than that predicted by another model. The Intergovernmental Panel on Climate Change (IPCC) reports suggest that the equilibrium climate sensitivity estimated from recent temperature change is 1.2K to 5.3K (5% significance level) under double CO_2 concentration (Bindoff et al. 2013), consistent with the model predicted values.

However, the uncertainty on equilibrium climate sensitivity estimated from observations is larger than the spread in climate models, so observations could not constrain the equilibrium climate sensitivity directly. Under such circumstances, we need to analyze the feedback processes in climate models and observations to evaluate the model predicted equilibrium climate sensitivity.

1.2 Climate feedbacks

The equilibrium climate sensitivity is decided by climate feedbacks. When there is a positive climate radiative forcing, the top of atmosphere (TOA) fluxes become imbalanced and there will be a change in mean surface temperature. Changes of mean surface temperature would result in changes in a certain variable, (such as cloud amounts, surface albedo, water vapor concentrations and thermal radiations), and the changed variable will results in an additional change in TOA flux, subsequently resulting a change in the surface temperature. This process is called climate feedback.

The magnitude of climate feedback from a certain type of variable X is defined as:

$$f_X = \frac{\partial R_X}{\partial X}\frac{dX}{dT_s}, \tag{1.2}$$

where R_X is the change of TOA flux induced by change of X, and T_s is the mean surface temperature.

When the surface temperature changes, the corresponding change in TOA flux is

$$dR = \sum_i f_{Xi} dT_s, \tag{1.3}$$

where f_{Xi} is the feedback of the ith component.

An equilibrium climate state is identified by zero net TOA flux. When a climate forcing F is introduced to an equilibrium climate system, there will be a rapid adjustment of air temperature, cloud, and water vapor (Vial et al.), then the TOA flux will change from 0 to $F+F_{adj}$, where F_{adj} is the forcing induced by rapid adjustment. The average temperature of the climate system changes in response to unbalanced TOA flux until the

climate system reaches a new equilibrium. Under the new equilibrium state, the net TOA flux is also zero, so

$$F + F_{adj} + \Delta R = F + F_{adj} + \sum f_{Xi} \Delta T_s = 0 , \tag{1.4}$$

where ΔR is the change of TOA flux after the forcing F is introduced, and ΔT_s is the change of equilibrium mean surface temperature. Then we get

$$ECS = \frac{\Delta T_s}{F} = -\frac{1 + F_{adj} / F}{\sum_i f_{Xi}} . \tag{1.5}$$

According to Equation (1.5), the equilibrium climate sensitivity is proportional to the reciprocal of the summation of all climate feedbacks.

The most important climate feedbacks are lapse rate feedback, Planck feedback, water vapor feedback, surface albedo feedback, and cloud feedback (Dessler 2013). Spread of lapse rate feedback, Planck feedback, water vapor feedback, and surface albedo feedback are small in climate models, and the uncertainty on cloud feedback is the primary contributor to the large spread of equilibrium climate sensitivity in climate models (Dessler 2010, 2013).

Therefore, study of cloud feedback is the key to evaluate the equilibrium climate sensitivity predicted by climate models.

1.3 Cloud feedback

Clouds cover about two-thirds of Earth's surface and substantially regulate Earth's radiation budget. They cool the planet by reflecting shortwave (SW; 0.2–4 μm) radiation back to space, and warm it by reducing outgoing longwave (LW; >4 μm) radiation (Figure 1.1). In the present climate, the SW effect dominates, so the net effect of clouds

is to cool the planet (e.g., Allan 2011). As the climate warms, the effect of clouds on the planet's radiation balance may also change, resulting in a feedback to the global climate system.

Many previous studies have examined the cloud feedback in general circulation models (GCM) in response to long-term global warming (Colman 2003; Soden and Held 2006; Dessler 2013), finding a cloud-feedback magnitude ranging from near 0 to 1.5 $W/m^2/K$. There are, however, few estimates from observations, mainly owing to the dearth of data of appropriate length and quality. Dessler (2010, 2013) used measurements of TOA flux from the Clouds and the Earth's Radiant Energy System (CERES) and estimated that the cloud feedback in response to short-term climate variations is positive and has a magnitude of 0.5 ± 0.8 $W/m^2/K$. Other studies have investigated regional cloud feedbacks in observations. Clement et al. (2009) used a cloud dataset from the northeastern Pacific to show that low clouds in that region acted as a positive feedback to multi-decadal regional surface temperature changes. The GCMs that best reproduced the cloud behavior in that region and on that time scale had average or stronger positive global cloud feedbacks in response to long-term global warming. Zelinka and Hartmann (2011) showed that high tropical clouds rose and contracted in area in response to inter-annual surface warming, leading to a net positive short-term cloud feedback from these types of clouds, although the cloud anomalies differed in subtle ways from those occurring under long-term warming.

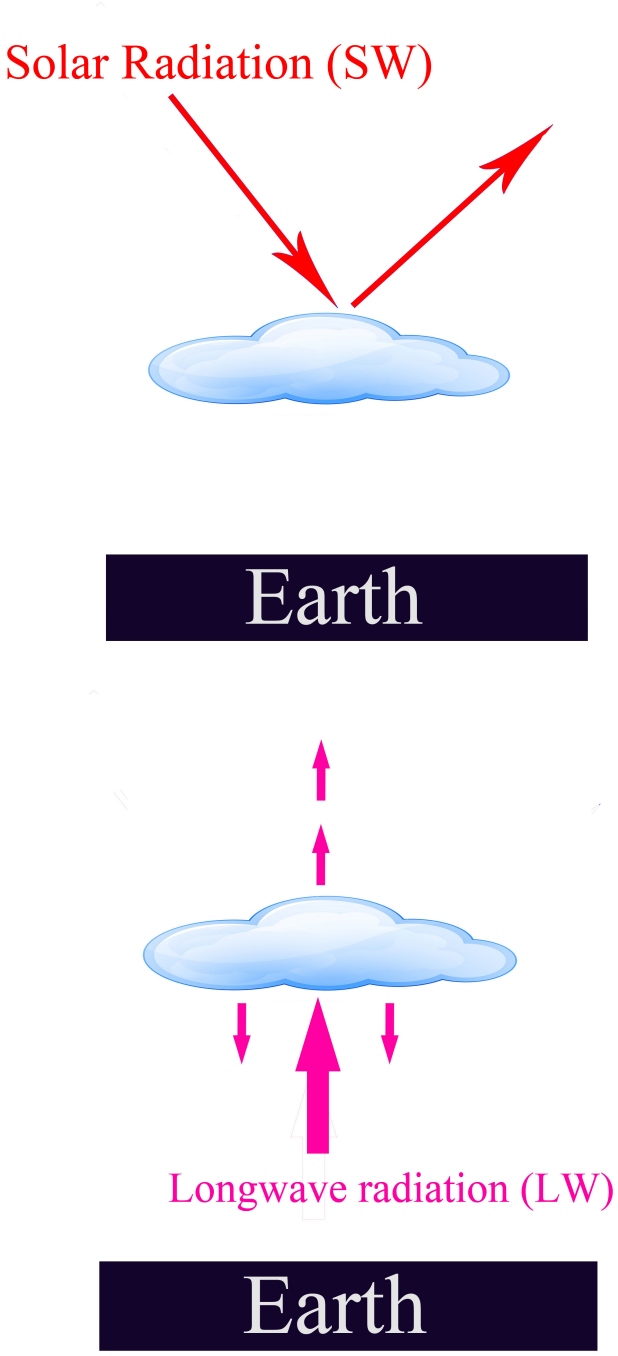

Figure 1.1 Clouds cool the planet by reflecting SW solar radiation back to the space, and warm the planet by reducing outgoing LW radiation.

Uncertainty on planetary boundary layer (PBL) clouds in GCMs is the primary source of the large spread in GCM predicted cloud feedbacks (Bony et al. 2005). Sherwood et al. (2014) established a relationship between GCM convective mixing and model predicted low-cloud feedback, and suggest an equilibrium climate sensitivity of more than 3 degrees based on observed convective mixing. However, GCMs fail to predict the observed relationship between low cloud fraction and estimated inversion strength (EIS) (Caldwell et al. 2013), and models may systematically overestimate the climate sensitivity.

To evaluate the cloud feedback in response to long-term climate changes (long-term cloud feedback) with observational short-term cloud feedback in response to climate fluctuations (short-term cloud feedback), it is necessary to establish a link between the short-term and long-term cloud feedbacks. However, there is no apparent relationship between the magnitude of short-term and long-term cloud feedbacks, and the spatial pattern of short-term and long-term cloud feedback is largely different (Dessler 2013). Therefore, an attribution analysis is applied in this study to find the underlying link between short-term and long-term cloud feedback.

In this thesis, we attribute the observed short-term cloud feedback with cloud kernel methods (Section 2), and analyze the cloud feedback in GCM simulations (Section 3). Subsequently we investigate the link between short-term and long-term cloud feedbacks (Section 3), and evaluated the long-term cloud feedback using observations (Section 4).

2. CALCULATE SHORT-TERM CLOUD FEEDBACK WITH OBSERVATIONS*

2.1 Data and methods

There are two methods to calculate cloud feedback.

The first method, which is referred to as "adjusted CRF method" in this thesis, is to calculate cloud feedback based on TOA radiative fluxes. The first step is to calculate the change of cloud radiative effect (CRE) in response to surface temperature change, and separate out the contribution of water vapor, temperature and surface albedo changes. Then the adjusted cloud radiative effect ΔR_{cloud} is calculated as (Soden et al. 2008):

$$\begin{aligned}\Delta R_{cloud} &= \Delta R_{allsky} - \Delta R_{clearsky} \\ &+(K_T^0 - K_T)\Delta T + (K_w^0 - K_w)\Delta W + (K_a^0 - K_a)\Delta a, \\ &+G^0 - G\end{aligned} \tag{2.1}$$

where ΔR_{allsky} is the change of all-sky (sky with clouds) TOA fluxes, $\Delta R_{clearsky}$ is the change of clear-sky (sky without clouds) TOA fluxes, ΔT is change of surface and air temperature, Δa is change of surface albedo, and ΔW is change in water vapor concentration. K_W, K_T, and K_a are all-sky radiative kernels of water vapor, temperature, and surface albedo, respectively; K_W^0, K_T^0, and K_a^0 are clear-sky radiative kernels of water vapor, temperature, and surface albedo, respectively. G is the total-sky forcing, and G^0 is the clear-sky forcing. Soden et al. (2008) estimated that G^0-G=0.16G. The short-term cloud feedback in response to inter-annual climate fluctuations is calculated as the regression slope of ΔR_{cloud} monthly anomalies against ΔT_s monthly anomalies.

*Parts of this section are reprinted from "An analysis of the short-term cloud feedback using MODIS data", by Zhou, C., M.D. Zelinka, A.E. Dessler, and P. Yang, 2013, J. Climate, 26, 4803-4815. ©American Meteorological Society. Used with permission.

Long-term cloud feedback in response to climate change is calculated as the long-term change of ΔR_{cloud} divided by the change of ΔT_s.

The second method is to calculate the cloud feedback using cloud histograms and cloud radiative kernels, and the method is referred to as "cloud kernels method" in this thesis. The first step of cloud kernels method is to calculate the so-called "cloud radiative kernels":

$$K(\tau, CTP) = \frac{\partial R_{cloud}}{\partial C}, \tag{2.2}$$

where R_{cloud} is the cloud radiative effect, τ is optical depth, CTP is cloud top pressure, and C is the cloud fraction. Then the change of cloud radiative effect can be estimated using the following equation:

$$\Delta R_{cloud} = K \Delta C . \tag{2.3}$$

Subsequently the short-term cloud feedback in response to inter-annual climate fluctuations could is calculated as the regress slope of ΔR_{cloud} monthly anomalies against ΔT_s monthly anomalies. Long-term cloud feedback in response to climate change is calculated as the long-term change of ΔR_{cloud} divided by the long-term change of ΔT_s.

2.2 Calculation of short-term cloud feedback with MODIS

In this subsection, observations are used to calculate cloud feedback with the cloud kernels method. Cloud observations made by the Moderate Resolution Imaging Spectroradiometer (MODIS) onboard NASA's Terra satellite (Platnick *et al.*, 2003) are used to calculate the cloud feedback of thick clouds. The monthly joint histograms of

cloud-top pressure and cloud optical depth provided in the MOD08 product (Hubanks *et al.*, 2008) covering the period March 2000 to February 2010 are used here. Figure 2.1(a) plots the average cloud fraction over this period in each CTP-τ bin.

The cloud radiative kernels have been calculated using a radiative transfer model by Zelinka *et al*. (2012a) and are updated here by replacing the GCM-mean temperature, water vapor, and ozone fields used as input to the radiation code with monthly-mean fields from the ERA-Interim Reanalysis (Dee *et al.*, 2011). The kernels are calculated separately for SW and LW fluxes, allowing it possible to additionally separate the cloud feedback into SW and LW components. The kernels are functions of *CTP*, τ, latitude and month; the SW kernels are also functions of clear-sky surface albedo. Before computing ΔR_{cloud}, at each latitude the SW kernels are mapped from surface-albedo space to longitude using monthly climatological surface albedo from the ERA-Interim Reanalysis.

Then the time series of $\Delta R_{cloud}(lon,lat,CTP,\tau)$ is regressed against the monthly global average surface temperature anomaly ΔT_s using an ordinary least-squares fit. The stated uncertainties in this study are the 95% confidence interval, calculated as twice the standard error of the slope of the fit. The GISS surface temperature data set (GISTEMP) (Hansen *et al.*, 2010) is used in this subsection.

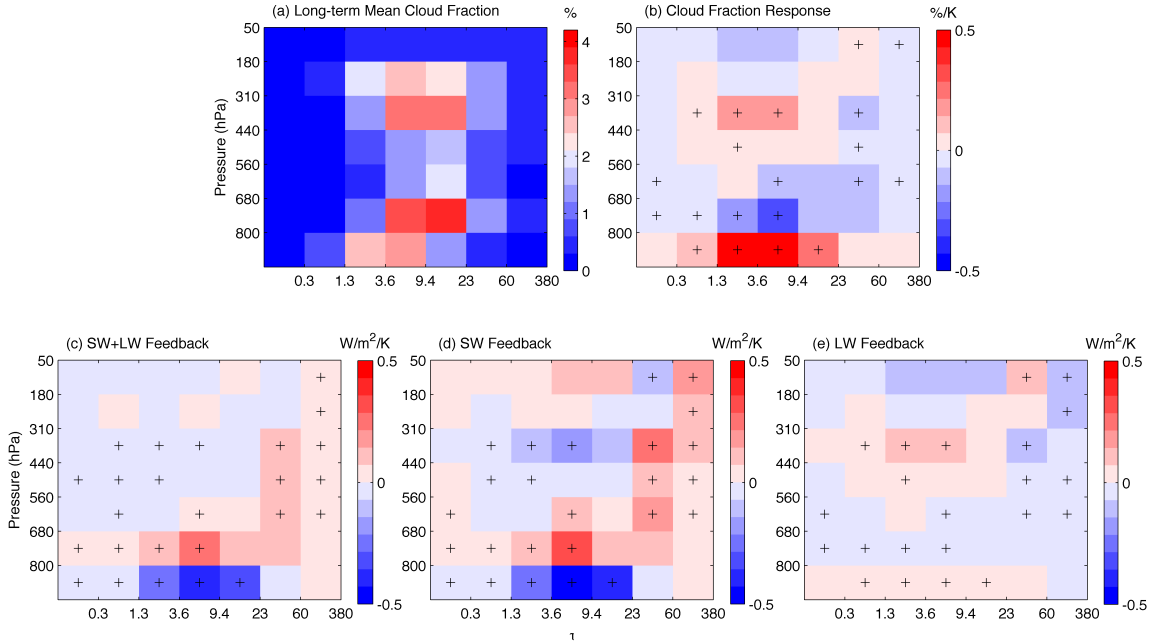

Figure 2.1 Short-term cloud feedback as a function of CTP and optical depth. (a) Average cloud fraction C in each each CTP-τ bin (%); integration over all bins yields 48%, the total cloud fraction in these histograms. (b) Slope of the regression of cloud-fraction anomaly ΔC in each bin vs. ΔT_s (%/K). (c-e) The contribution to the net cloud feedback, SW cloud feedback, and LW cloud feedback, respectively, in W/m^2/K. Note that the multiplication of cloud radiative kernels with cloud fraction anomalies occurs at every location and is then spatially averaged for display in this figure. In all panels, the x-axis is optical depth, and the y-axis is cloud-top pressure. Bins where the regression slope is statistically significant (>95%) are marked with black crosses.

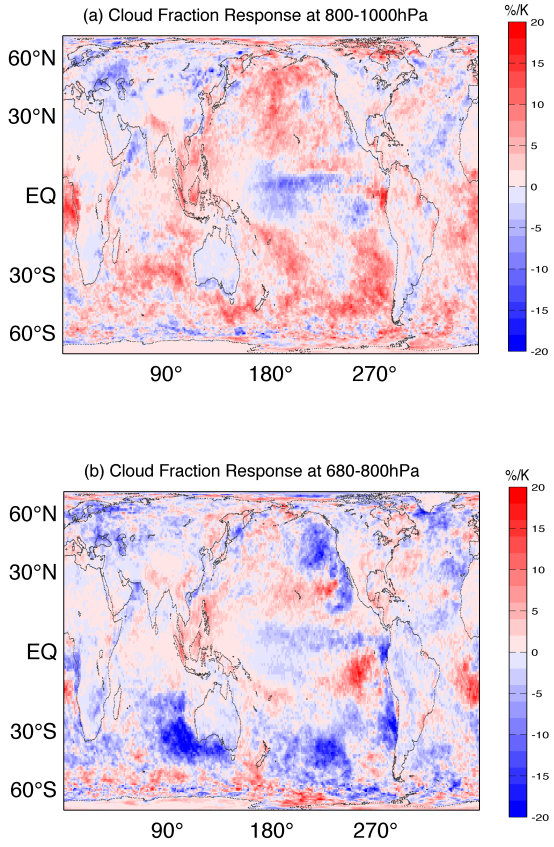

Figure 2.2 Low cloud fraction response to inter-annual surface warming (%/K). (a) the 1000-800 hPa layer and (b) the 800-680 hPa layer. The y-axis in these plots is area-weighted latitude.

Table 2.1 Summary of short-term cloud feedbacks. All values have units of $W/m^2/K$; uncertainties are $\pm 2\sigma$. Source of ΔT_s data: GISTEMP (Hansen et al. 2010); Hadley Centre/Climatic Research Unit, version 4 (HadCRUT4; Morice et al. 2012); ERA-Interim (Dee et al. 2011); the National Climatic Data Center (NCDC; Smith et al. 2008); and NASA's MERRA (Rienecker et al. 2011).

MODIS global-average cloud feedback	SW	LW	Net (LW+SW)
ΔT_s dataset:			
GISTEMP	+0.47±1.02	-0.48±0.68	-0.02±0.76
HadCRUT4	+0.50±1.20	-0.53±0.80	-0.03±0.90
ERA-interim skin temperature	+0.35±1.01	-0.45±0.68	-0.10±0.76
NCDC	+0.35±1.25	-0.58±0.84	-0.23±0.94
MERRA skin temperature	-0.17±1.02	-0.28±0.69	-0.45±0.76
CERES global-average cloud feedback			
Average of values in Table 1 of Dessler and Loeb (2012) (Terra period)	+0.14±0.78	+0.43±0.47	+0.57±0.71

Figure 2.1(b) shows the slope of the linear regression of global average ΔC vs. ΔT_s in each CTP-τ bin. The largest positive slopes (i.e., ΔC increasing with increasing ΔT_s) are found in the lowest pressure bins (pressure > 800 hPa), with large negative slopes in the bins above (800-680 hPa). Figure 2.2 shows the spatial distribution of the correlations in the 1000-800 and 800-680 hPa layers. Both layers show that the dominant response of clouds is over the oceans. In the 1000-800 hPa layer, positive correlations exist over wide areas of the oceanic subtropics and mid-latitudes. In the 800-680 hPa layer, the dominant correlations are more localized and negative, and primarily located over the ocean to the west of N. and S. America and Australia.

Figures 2.1(c), 2.1(d), and 2.1(e) show the net, SW and LW cloud feedbacks, respectively, in each CTP/optical depth bin. Summing the bins each panel yields the respective global cloud feedbacks, and these values are summarized in Table 2.1. As pointed out by Dessler and Loeb (2013), and confirmed here, the choice of ΔT_s dataset can have a significant impact on the calculated cloud feedback. Aside from the Modern-Era Retrospective Analysis for Research and Applications (MERRA), all of the calculations produce slightly negative net feedbacks (although statistically indistinguishable from zero), which arise from a combination of a positive SW feedback and a larger negative LW feedback. The MERRA seems to be an outlier in this regard—it predicts both a negative SW and LW feedback. It is unclear why the MERRA result stands out, although given the uncertainty in the fits, it could just be a statistical fluctuation. Averaging all of the calculations together and combining the uncertainties in quadrature, the SW, LW, and net cloud feedbacks are +0.30±1.10, -0.46±0.74, and -0.16

±0.83 W/m^2/K (excluding the MERRA results yields values of +0.42±1.13, -0.51±0.75, and -0.10±0.84 W/m^2/K). All subsequent calculations in this subsection use the GISTEMP ΔT_s dataset (Hansen et al. 2010).

Also listed in Table 2.1 are the cloud feedback values calculated using CERES measurements (Dessler 2010, 2013). The CERES measures the TOA net flux, and the CERES cloud feedbacks are calculated from the adjusted CRF method, so the values are completely independent of the MODIS values, and the comparison provides an important test of the MODIS results. In the CERES data, both the SW and LW feedbacks are positive, but the relative magnitudes differ depending on the reanalysis data set used in the calculation. The MODIS SW cloud feedback is 0.16-0.28 W/m^2/K larger than the CERES SW cloud feedback, while the MODIS LW cloud feedback is ~9 W/m^2/K smaller than the CERES estimate. This leads to the net cloud feedback from MODIS observations being ~0.7 W/m^2/K smaller than that from the CERES observations—a big enough difference that the net feedback in the MODIS and CERES calculations have different signs

The main difference between the net cloud feedback estimates is a lower value of the LW cloud feedback from MODIS. Some of the difference can be explained by the method: Zelinka *et al*. (2012a) found that, in an analysis of GCMs, the cloud-kernel-derived LW cloud feedbacks were on average 0.15 W/m^2/K lower than those computed using the adjusted ΔCRF method.

Limitations in the MODIS data may also contribute to the discrepancy. First, the optical depth of thinner clouds are not retrieved by MODIS (e.g., Marchand et al., 2010).

This includes about 20% of the pixels identified as cloudy by the MODIS cloud mask but for which the optical depth retrieval fails as well as clouds too thin to be flagged by the cloud mask ($\tau \approx< 0.3$). This is reflected in Figure 2.1(a), which shows few thin clouds, although other data show the clouds are indeed there (Dessler and Yang, 2003). Feedback from thin cirrus clouds is an important part of cloud feedback, and it is discussed in Section 2.3. Second, MODIS optical depth is retrieved using a bi-spectral method involving both visible and near-infrared bands (King *et al.*, 1992), so the MODIS data exclude nighttime regions, including the wintertime high latitudes. Both of these issues will lead to a bigger impact on MODIS's LW cloud feedback than the SW feedback.

Another potential problem is a mismatch in the MODIS retrieval between CTP and optical depth. For example, MODIS can correctly identify the CTP of an optically thin high cloud over a thick lower cloud, but the retrieved optical thickness is for the whole column. This would produce the wrong LW TOA flux anomaly when the retrieved properties of this cloud are multiplied by the LW cloud kernels.

The CERES-derived global average cloud feedbacks also have uncertainties. In addition to the uncertainty in the CERES measurements, the radiative kernels used to convert the CERES measurements to ΔR_{cloud} (Soden *et al.*, 2008; Shell *et al.*, 2008) are derived from GCMs, so may not completely represent reality. Nevertheless, in comparing the uncertainties, it is likely that the global-average cloud feedback from CERES may be more accurate than the values obtained from the MODIS measurements.

To further compare the MODIS and CERES cloud feedback calculations, Figure 2.3 shows the spatial distribution of SW cloud feedback calculated from MODIS observations. Regions that contribute positively (negatively) to the cloud feedback are colored red (blue). The El Nino/La Nina Southern oscillation (ENSO) is the dominant factor for the inter-annual climate variations over the period analyzed, and therefore the regional distribution of cloud feedback reflects a characteristic dipole pattern in the tropical Pacific.

Figure 2.3(b) shows the spatial distribution of the SW cloud feedback calculated from CERES observations. The difference between the MODIS and CERES cloud feedback estimates are in Figure 2.3(c). Clearly, the results calculated from MODIS agree well with that of CERES, capturing both the broad features and the detailed spatial structures of the cloud-induced TOA flux anomalies.

Figure 2.3(d) and 2.3(e) show the spatial distribution of the LW cloud feedback calculated from MODIS and CERES observations. The LW feedback is essentially a mirror image of the SW feedback, a consequence of the prominent role of high cloud anomalies in causing the radiative anomalies and their opposing SW and LW effects on climate. The difference is plotted in Figure 2.3(f), and once the difference is small compared to Figures 2.3(d) and 2.3(e).

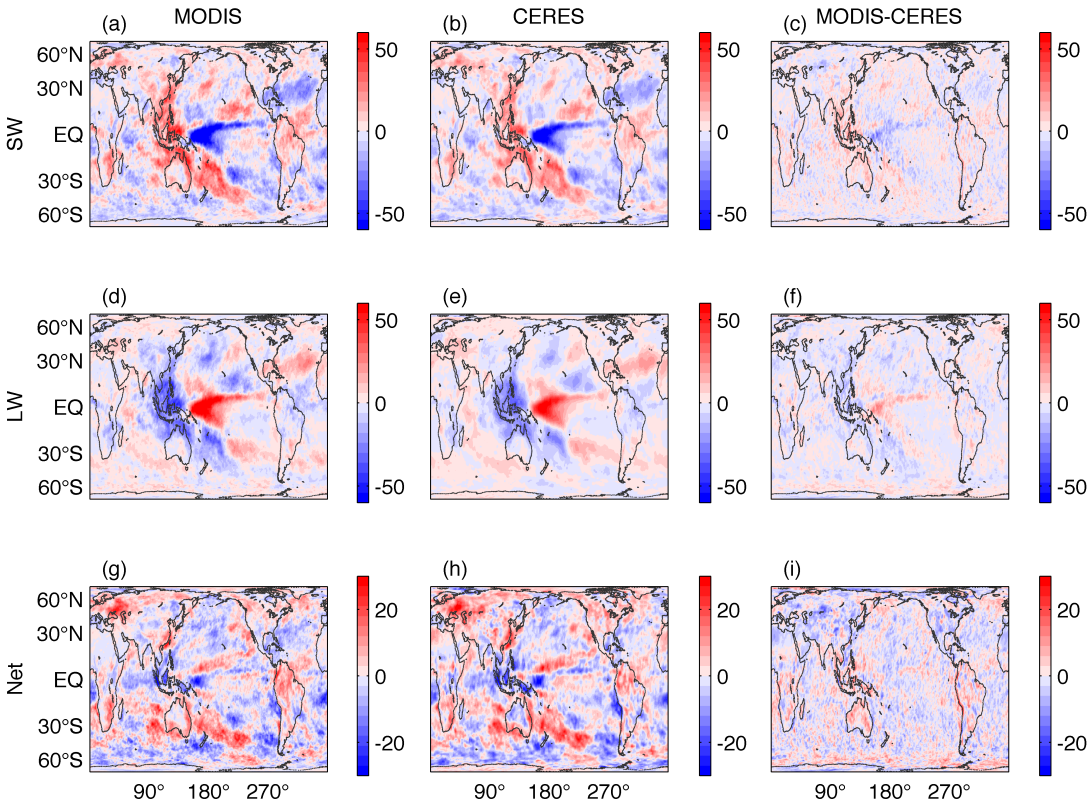

Figure 2.3 Spatial distribution of the short-term cloud feedback ($W/m^2/K$) calculated from MODIS observations (left panels) and CERES (middle panels), and the difference (MODIS minus CERES). (a-c) are the SW component of cloud feedback, (d-f) are for LW cloud feedback, and (g-i) are for net cloud feedback. The CERES ΔR_{cloud} values are from Dessler (2010, 2012). The y-axis in these plots is area-weighted latitude.

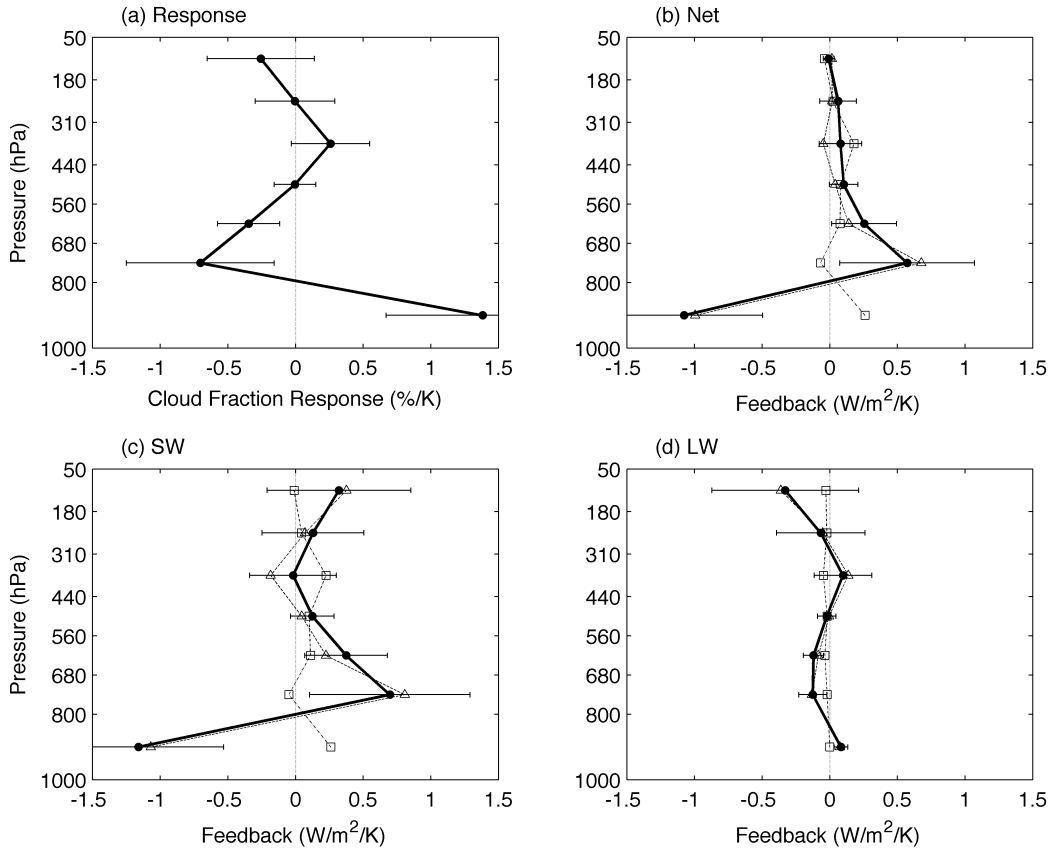

Figure 2.4 Vertical profile of short-term cloud feedback. (a) Altitude profile of the change of global mean cloud fraction per degree of global mean surface temperature anomaly (%/K). (b-d) The heavy line shows the contribution to the net, SW, and LW cloud feedbacks, respectively. The error bars indicate the 95% confidence interval. The lines with square and triangle symbols are the contributions to the cloud feedback at each altitude from changes in τ and cloud fraction.

Figures 2.3(g) and 2.3(h) show the net cloud feedback. Figure 2.3(i) shows the difference in the net feedback, and once again the values are small compared to Figure 2.3(g) and 2.3(h). This agreement is particularly notable since the net feedback is a small residual of two large but oppositely signed terms. Small errors in either the LW or SW term would lead to large errors in the net feedback — the lack of large errors increases our confidence in the cloud feedback calculations. The agreement also means that the differences in the global average feedbacks in Table 2.1 arise from small but widely distributed differences between the two calculations.

Figure 2.4 shows the cloud feedback as a function of cloud-top pressure, calculated by summing the bins in the panels in Figure 2.1(b-e) across optical depth. Figure 2.4(a) shows the slope of the regression between $\Delta C(CTP)$ vs. ΔT_s — it shows the biggest cloud changes occur for CTP above (altitudes below) 800 hPa. This layer by itself drives a net global cloud feedback of -1.08±0.58W/m^2/K (Figure 2.4b).

At pressure below (altitudes above) 800 hPa, changes in clouds produce a weakly negative LW cloud feedback (Figure 2.4d) and a strongly positive SW cloud feedback (Figure 2.4c), leading to a net positive feedback of +1.06±0.69 W/m^2/K (Figure 2.4b). Thus, the net global cloud feedback of about -0.02 W/m^2/K is set by a negative feedback due to clouds near the surface and a slightly smaller positive feedback due to clouds in the rest of the troposphere. Individually, both changes are statistically significant, but the smaller net cloud feedback is not.

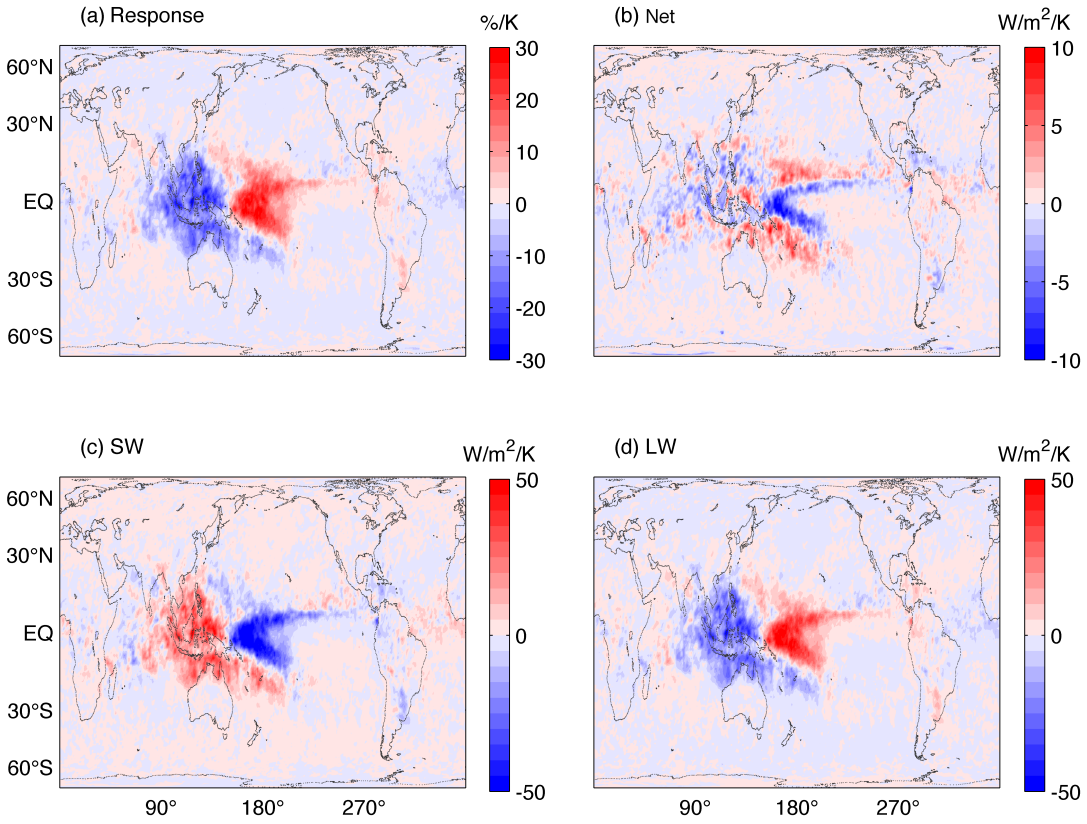

Figure 2.5 Short-term high cloud feedback. (a) Slope of the regression of cloud fraction vs. ΔT_s (%/K) for the 180-50 hPa layer. (b-d) The contribution of cloud changes in this layer to the net, SW, and LW cloud feedbacks, respectively. The y-axis is area-weighted latitude.

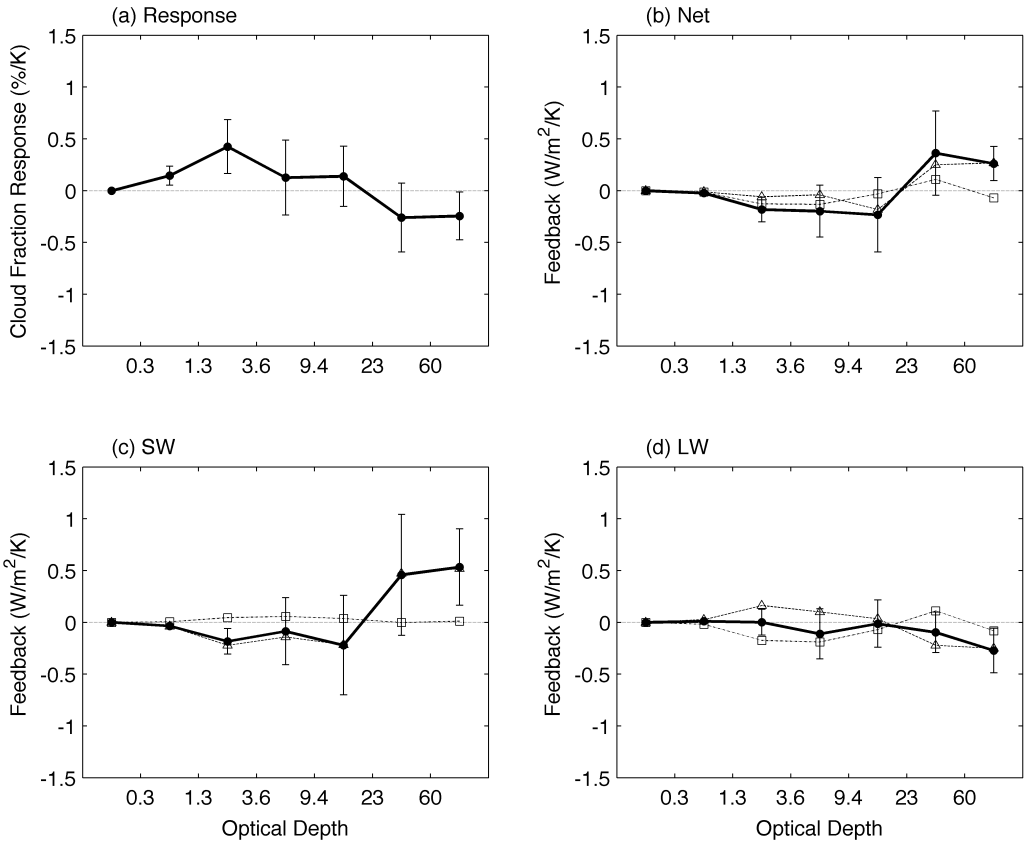

Figure 2.6 Short-term cloud feedback as a function of optical depth. (a) Slope of the regression of cloud fraction vs. ΔT_s (%/K), as a function of cloud optical depth. (b-d) The heavy line shows the contribution to the net, SW, and LW cloud feedbacks, respectively. The error bars indicate the 95% confidence interval. The lines with square and triangle symbols are the contributions to the cloud feedback at each altitude from changes in cloud height and cloud fraction.

The largest LW cloud feedbacks are found in the uppermost bins, covering CTP of 180-50 hPa. This makes sense since these clouds provide the largest temperature contrast with the underlying surface. The LW feedback there is negative and it plays a dominant role in producing the overall negative global LW cloud feedback. Figure 2.5 shows the spatial distribution of the cloud changes and the associated feedbacks in the uppermost layer. This figure shows a classic ENSO dipole response of cloud fraction changes in the tropical Pacific. It is also clear that the resulting LW and SW feedbacks substantially cancel each other — not just in the global average, but also at individual grid points.

Averaging over the entire 180-50 hPa layer, cloud changes that drive the negative LW feedback generate an almost equivalent but oppositely signed SW cloud feedback (Figures 2.4c and 2.4d). The net cloud feedback at these altitudes is therefore close to zero (Figure 2.4b). Figure 10 and Table 1 of Zelinka and Hartmann (2011) show a similar amount of cancellation between LW and SW fluxes due to cloud anomalies in the upper troposphere, although that study focused on the tropics. Loeb *et al*. (2012) also found a negative LW and positive SW tropical cloud feedback response to ENSO.

Figure 2.6 shows the feedback as a function of cloud optical depth, calculated by summing the bins in Figure 2.1(b-e) across CTP. The fraction of clouds with $\tau \geq 23$ decreases with increasing ΔT_s, while the fraction of thinner clouds increases (Figure 2.6a). The increase in thin clouds at the expense of thick clouds leads to a positive SW cloud feedback and a smaller negative LW cloud feedback.

In the net, Figure 2.6(b) shows that the near-zero net cloud feedback comes from a positive cloud feedback from decreasing thick cloud frequency and a negative feedback

from increasing thinner clouds. The thinnest clouds contribute little to the net feedback, although, as mentioned previously, this might be a consequence of MODIS's inability to retrieve cloud properties for these clouds.

Figure 2.7 compares the SW, LW, and net cloud feedback derived from MODIS and CERES as a function of latitude. The SW feedback shows excellent agreement at all latitudes — the largest difference is at 15°N and 15°S, where the MODIS-derived feedback is larger than that from CERES, and it is these differences that are mainly responsible for MODIS's slightly larger SW cloud feedback. In the LW, the cloud feedback derived from CERES is more positive than the MODIS feedback at almost all latitudes. Integrating over the globe, this small difference at each latitude sums to produce the large underestimate of the global LW cloud feedback by MODIS discussed previously.

Figure 2.7 also plots the net cloud feedback vs. latitude. There is excellent agreement between the MODIS and CERES net cloud feedbacks. This means that most differences between CERES and MODIS in the LW cloud feedback are canceled by compensating differences in the SW feedback. The exception is between 20°N and 60°N, where the CERES net cloud feedback is higher than MODIS. This difference leads to the difference in the overall net cloud feedback between these two data sets. It is presently unknown why the datasets disagree over these latitudes.

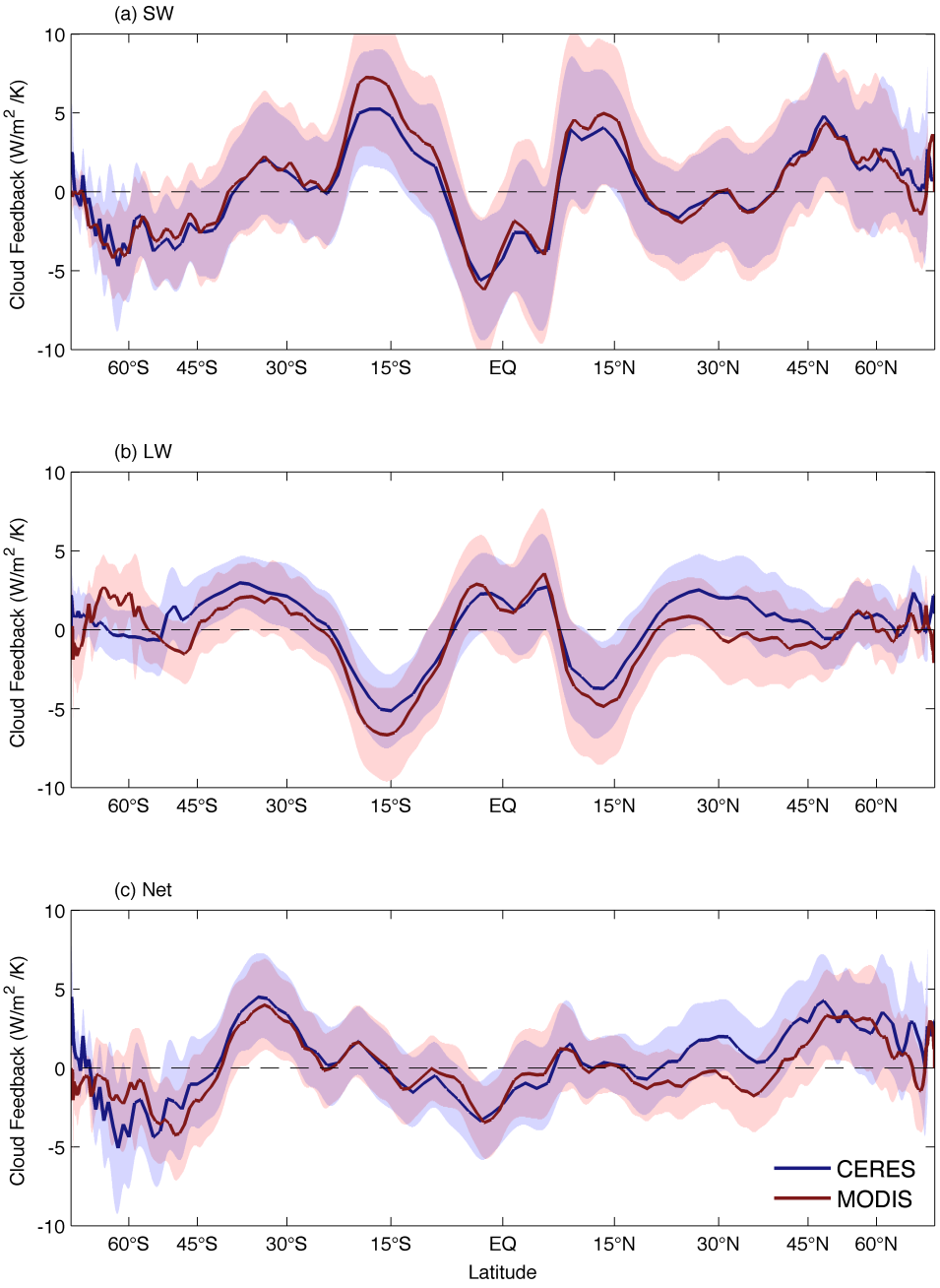

Figure 2.7 The zonal mean short-term cloud feedbacks. The red line is the cloud feedback calculated from MODIS, and the red shading represents the 95% confidence range. The blue line is the feedback from CERES (Dessler, 2010; 2012), and the blue shading represents the 95% confidence range (where they overlap, the shading is purple).

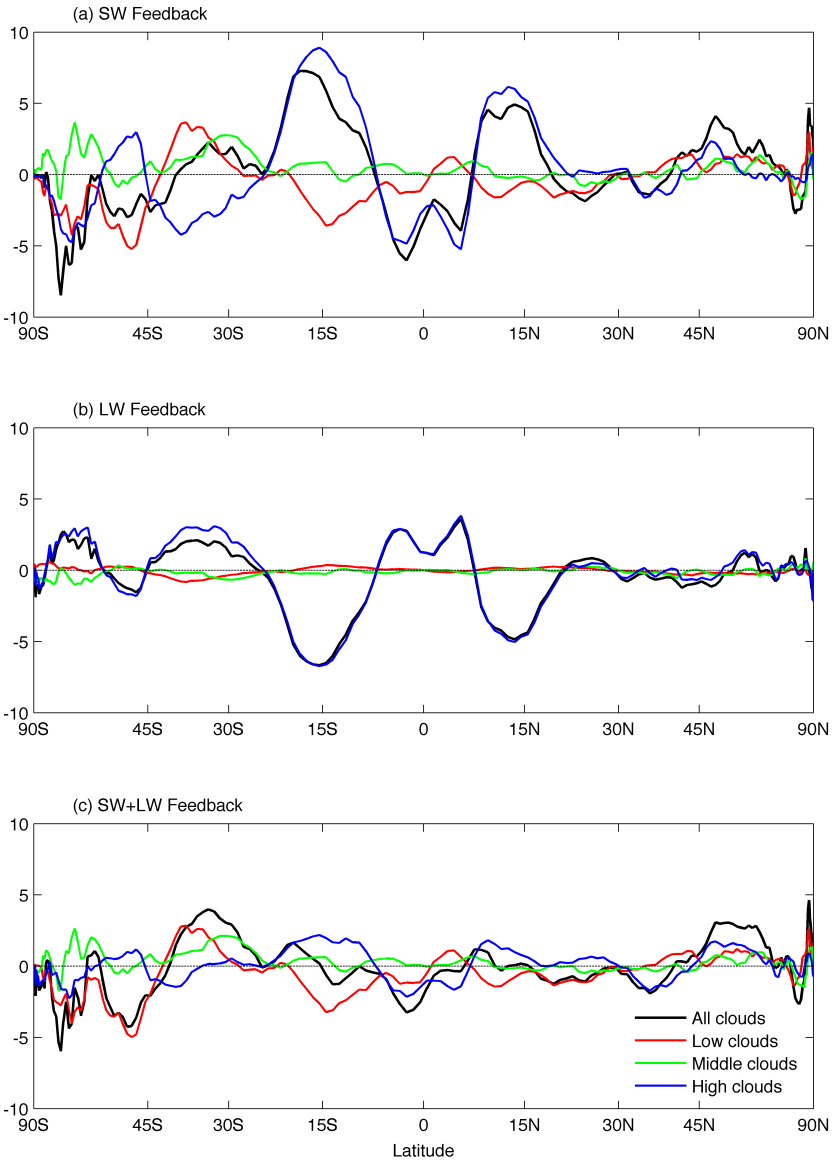

Figure 2.8 The zonal mean short-term cloud feedbacks for low, middle and high clouds. The black solid line is the total cloud feedback calculated from MODIS. The blue, green, and red lines represent high (CTP < 440 hPa), mid-level (440 < CTP < 680 hPa) and low clouds (CTP > 680 hPa).

The latitudinal pattern of the LW and SW cloud feedbacks in Figure 2.7(a) and 2.7(b) primarily reflects the equatorward shift of the subtropical jets during the El Nino phase of ENSO (Trenberth and Hurrell, 1994). This shifts the cloudy regions onto the Equator and the clear subtropics towards the equator — and results in the hemispherically symmetric pattern in the Tropics evident in Figure 2.7. Because the cloud changes are primarily driven by rearrangements in the atmospheric circulation, a large positive LW cloud feedback at one latitude will tend to be cancelled in the global average by a large negative LW cloud feedback at another latitude. This also applies for the SW cloud feedback. As a result, the global average feedbacks listed in Table 2.1 are small residuals of the large and offsetting feedbacks at different latitudes.

Figure 2.8 shows the latitudinal distribution of the cloud feedback broken down into high, mid-level, and low clouds. The SW cloud feedback is dominated in the tropics by high clouds; in the extratropics, clouds at all heights become important. The LW feedback is dominated by high clouds at almost all latitudes. Table 2.1 lists the global average cloud feedback from the three cloud heights. About 60% of the global LW cloud feedback is due to high clouds, with most of the remaining negative feedback coming from mid-level clouds. The global SW feedback is set by a positive cloud feedback from mid- and high clouds, which is reduced by about 50% by a negative feedback from low clouds.

In the net, Figure 2.8 shows that the SW and LW effects of high clouds tend to cancel, leading to a much smaller net cloud feedback for these clouds at most latitudes. Mid- and low-altitude clouds experience less cancellation between their SW and LW

components. The result is that clouds at all levels play equally important roles in the latitudinal distribution of the net cloud feedback.

The MODIS ΔR_{cloud} vs. GISTEMP ΔT_s plot is shown in Figure 2.9(a) (slope = -0.02±0.76 W/m2/K). The correlation between these variables is poor and the scatter in the data results in a highly uncertain cloud feedback. One might conclude from this that clouds are only weakly impacted by ΔT_s variations.

Analysis of the MODIS data helps us further refine our understanding of this issue. Figure 2.9(b) shows a scatterplot of ΔR_{cloud} vs. ΔT_s for the lowest layer (1000-800 hPa) (slope = -1.08±0.58 W/m2/K) and Figure 2.9(c) shows the same thing for the rest of the troposphere (800-50 hPa) (slope = +1.06±0.69 W/m2/K). Both relations are statistically significant (although there is still considerable scatter), so one can conclude that clouds in these layers are indeed related to ΔTs. The relationships have opposite signs, however, so when one considers the entire troposphere (Figure 2.9a), they cancel and no clear relation exists.

This can also be seen in Figure 2.1(b-e), in which CTP-τ bins that show statistically significant correlations with ΔTs are marked with a cross. About 40-50% of the bins show statistically significant relations (more than would be expected due to chance), confirming in more detail the results in Figure 2.9.

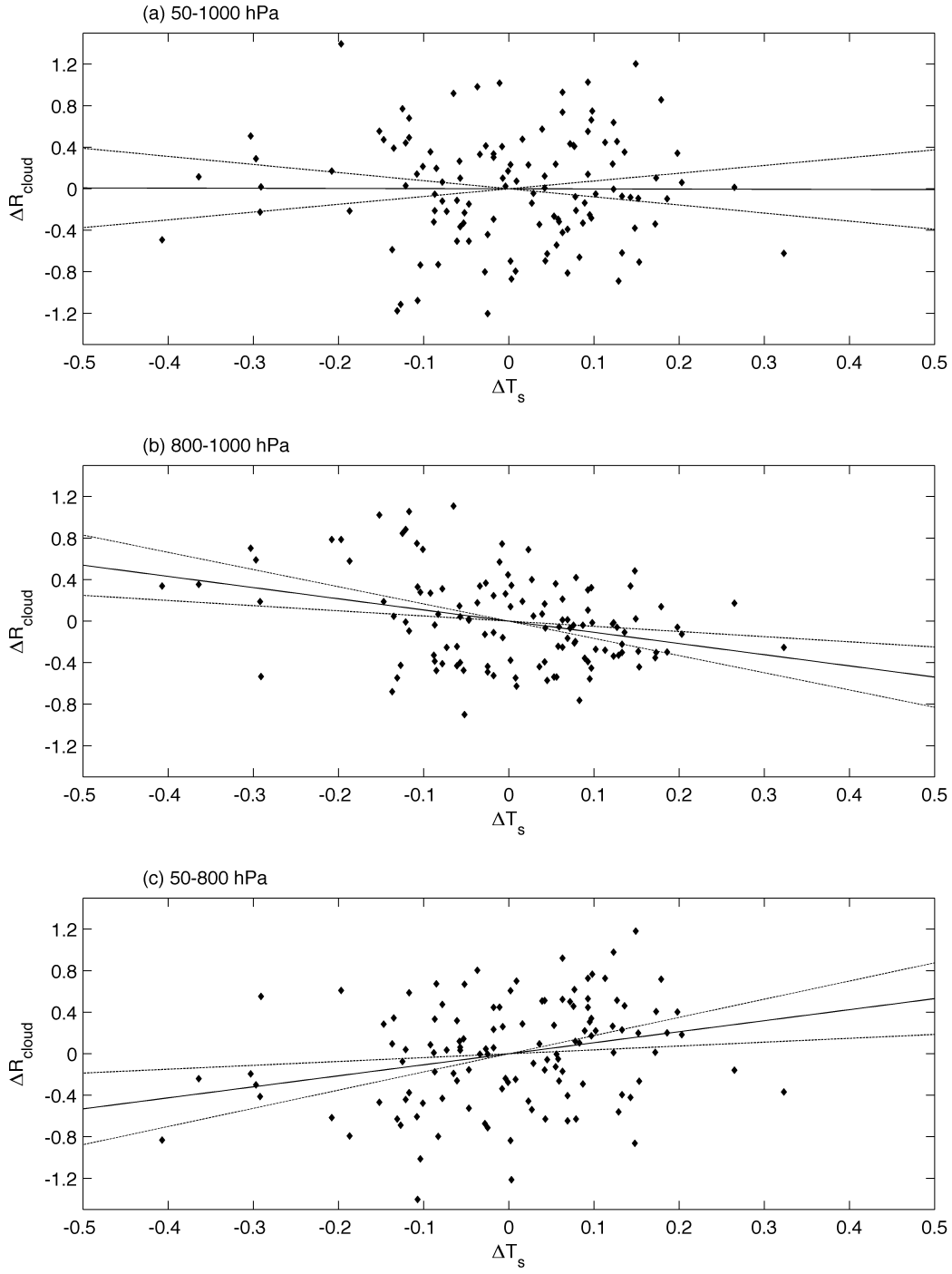

Figure 2.9 Comparison of ΔR_{cloud} vs. $\Delta T_{s.}$ (a) the global average 1000-800 hPa layer, (b) the 800-50 hPa layer, and (c) the entire column (1000-50 hPa). The least-squares fit and the 2σ uncertainty of the fit are also shown.

This reflects a general truth about these data: the global average cloud feedback is a small residual of the sum of larger and often statistically significant quantities that oppose each other horizontally, vertically, in optical depth space, and spectrally (LW vs. SW). Thus, it is not correct to conclude, on the basis of a plot like Figure 2.9(a), that ΔT_s has little influence on clouds. Rather, individual cloud populations may indeed be controlled by ΔT_s, but cancellations in the global average calculations obscure the relationships.

Much of this cancellation may be due to the fact that the climate variation we are using to extract the cloud feedback is ENSO, which is a large-scale rearrangement of the atmospheric circulation. This rearrangement leads to large but compensating changes in clouds, and therefore to the cancellation identified above. GCM simulations of long-term global warming show a more uniform response, with both the LW and SW feedback being positive at most latitudes (e.g., Dessler, 2012, Figure 6; Zelinka et al., 2012a, Figure 6).

MODIS does not contain most of the thin clouds, so the feedback from cirrus clouds is not included, which is an important part of cloud feedback and may partially explain the difference between MODIS and CERES. In this case, we calculated the cirrus feedback using Cloud-Aerosol Lidar and Infrared Pathfinder Satellite Observation (CALIPSO) cloud layer products.

2.3 Calculation of cirrus feedback with CALIPSO

Cirrus clouds, a genus of thin and wispy high clouds covering about 20% of the earth's surface (Liou 1986), are among the principal cloud types controlling the Earth's

radiation budget (Lynch, 1996). Cirrus clouds heat our planet by reducing outgoing LW radiation more than they reduce incoming SW solar radiation. As the global surface temperature rises, changes in cirrus amount, optical depth, and altitude may further alter the earth's energy budget, resulting in a feedback to the climate system. As is discussed in Section 2.2, MODIS has difficulty retrieving the properties of thin cirrus, especially in regions of broken cloudiness or near the edge of clouds (Marchand et al. 2010; Pincus et al. 2012). This motivates us to better quantify the role of cirrus clouds in the short-term climate fluctuations.

While the warming effect of cirrus clouds in the current climate has been widely realized, the role of changing cirrus in climate changes has not been reliably quantified. Based on thermodynamic arguments, Liou (2005) suggested that cirrus clouds would produce a positive feedback through rising in a warmer atmosphere. Cirrus clouds in climate models could exert a positive feedback (Zelinka et al. 2012), but the extent has not been reliably quantified by climate models (Liou, 2005). On the other hand, most satellite datasets do not contain reliably retrieved optical properties of thin cirrus clouds, and the cirrus feedback has not been quantified using observations

The CALIPSO level-2 1-km cloud layer product (Winker et al. 2003) is used to quantify the cirrus feedback in response to interannual surface temperature anomalies. Measurements from December 2007 to August 2013 were obtained from the NASA Langley Research Center Atmospheric Science Data Center; the off-nadir angle of the lidar is 3° during this period, allowing us to avoid complications from horizontally

oriented crystals (Zhou et al. 2012, 2013). We calculate the optical depth (τ) of cirrus clouds using the formulation (Josset et al. 2012):

$$\tau = -\frac{1}{2\eta}\ln(1-2\eta S\gamma'), \tag{2.4}$$

where γ' is the layer-integrated backscatter of cirrus, S is the cirrus lidar ratio, and η is the multiple scattering factor. Following Josset et al. (2012), we use S = 33 sr and η = 0.61. The variations of lidar ratio and multiple scattering factor are small in cirrus clouds, and retrieved optical depth is accurate to construct optical depth histograms in this study. This process is similar to the cloud extinction retrieval in CALIOP operational product (Young and Vaughan, 2009).

We produce a joint histogram from the optical depth and CTP provided in the CALIPSO data. We limit our analysis in this paper to cirrus clouds with CTP less than (altitudes above) 440 hPa and that are not opaque to the laser (i.e., lidar signals can be detected below the high cloud layer, which typically requires $\tau < 3.5$ for cloud layers above the 440-hPa pressure level). This classification criterion is consistent with the International Satellite Cloud Climatology Project (ISCCP) cirrus cloud classification (CTP < 440hPa, $\tau < 3.6$).

CALIPSO sees multiple cirrus cloud layers frequently above 440 hPa, and we combine multiple cirrus cloud layers in each pixel into a single effective cloud layer that has the following properties:

$$\tau = \sum \tau_i \text{, and } CTP = \sum (CTP_i \times \gamma'_i) / \sum \gamma'_i \text{,} \tag{2.5}$$

where γ'_i, τ_i and CTP_i are the layer-integrated backscatter, optical depth and cloud top pressure for the i'th cirrus cloud layer, respectively. Our calculations show that the cloud radiative effect of the effective cloud layer is close to that of the multiple cirrus cloud layers, so we use the single-level effective cloud layer in the production of the CTP-τ histograms. For high cirrus clouds overlaying an opaque (tau > 3.5) high (altitude above 440 hPa) cloud, the effective cloud layer is also opaque, and is therefore not classified as cirrus clouds in this study. Such a situation occurs over only 1% of the planet, so few cirrus clouds are eliminated because of this. Thin cirrus layers that lie above opaque mid- and low-level clouds are included in this study, as discussed below.

To quantify the radiative feedback of cirrus, we also use the cloud kernels method. We calculate a set of cloud radiative kernels for cirrus clouds, which quantify the change in top-of-atmosphere (TOA) flux per percent change in cirrus cloud fraction with a particular CTP and τ:

$$K = \partial R / \partial C = (R_c - R_{nc}) / 100\% , \tag{2.6}$$

where R_c and R_{nc} is the TOA flux for sky with 100% cirrus coverage and without any cirrus, respectively. The kernel calculations follow Zelinka et al. (2012), except that the input zonal mean temperature, ozone, and water vapor fields are monthly mean fields from ECMWF Re-Analysis Interim. Because cloud particle size is smaller in colder clouds, we set the input effective particle diameter to be a function of cloud top temperature using the lookup table of Donovan (2003). Following Zelinka et al. (2012), the Fu-Liou model (Fu and Liou 1992) is used to perform the calculations.

The radiative kernels are then multiplied by the interannual anomalies in cirrus cloud fraction to get an estimate of the contribution of each cloud type to the change in TOA radiation, ΔR_{cloud}. The cirrus feedback is then calculated by regressing the anomaly of ΔR_{cloud} against the global surface temperature anomaly.

One challenge is to correctly handle thin cirrus over middle and low thick clouds. To do this, we calculate three sets of kernels: high cirrus over clear skies, high cirrus over a mid-level cloud, and high cirrus over a low cloud. For cirrus cloud layers without any underlying cloud layers, we follow the calculations of Zelinka et al. (2012). Figures 12.10 (a-c) show the globally averaged cirrus radiative kernels for cirrus cloud layers without any cloud layers below. Cirrus clouds generally have a warming effect on the planet.

To generate the kernel for cirrus layers above low-cloud layers (CTP>680hPa), a liquid cloud layer (τ=5, CTP=850 hPa) is inserted into the radiative transfer calculations with and without cirrus. Figures 2.10 (d-f) show these kernels. The low-cloud layer also reflects SW solar radiation, so the SW radiative effect of cirrus is less negative than cirrus above clear-sky. On the other hand, the LW component of radiative effect for cirrus above low-cloud layers – which have little TOA LW impact – is similar to that for cirrus over clear skies, so the net radiative effect is these clouds show stronger heating. These calculations are analogous to those performed in generating the kernels over a range of surface albedos, as is done in Zelinka et al. (2012).

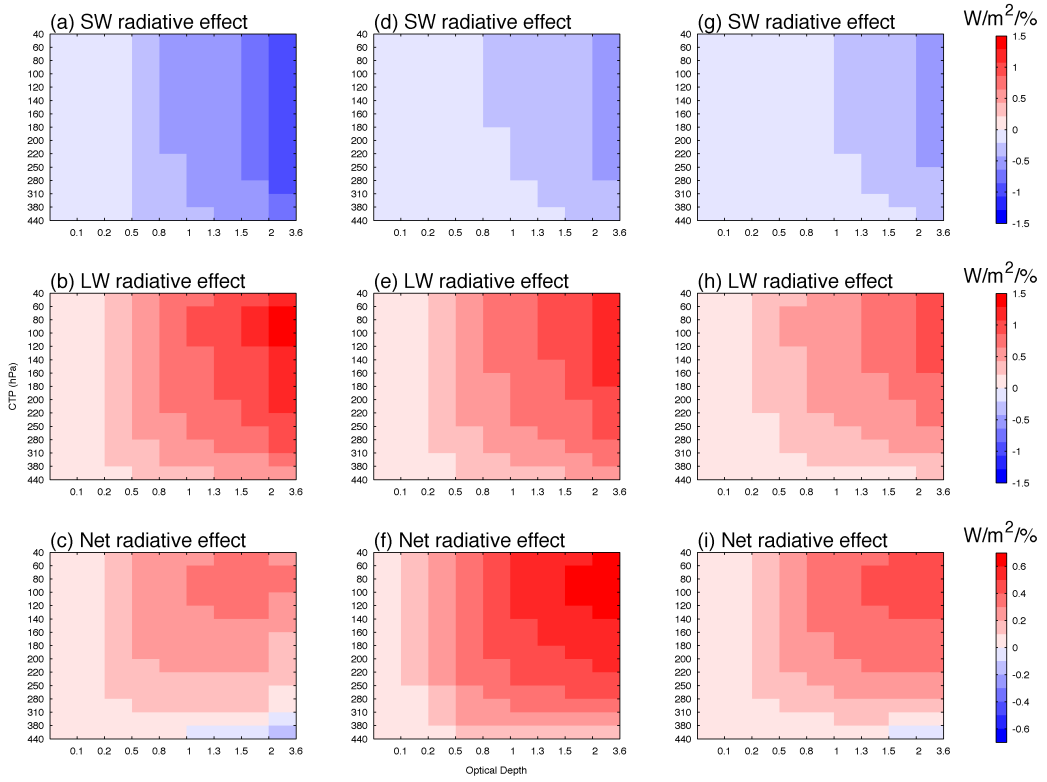

Figure 2.10 Cloud radiative kernels for cirrus clouds. (a-c) over clear skies, (d-f) over a single low-cloud layer, and (g-i) over a single mid-cloud layer. The upper panels are for the SW component, the middle panels are for LW component, and the bottom panels are the net (SW+LW) cloud radiative kernels.

For cirrus layers above mid-cloud layers (440hPa<CTP<680hPa), a liquid cloud (τ=5, CTP=550 hPa) is inserted into the kernel calculations. Figures 2.10(g-i) show the kernels for cirrus above middle cloud layers. The SW radiative effect is similar to cirrus above low clouds, but the LW effect is reduced significantly because mid-level clouds are colder than low clouds, so the net cloud radiative heating is weaker than cirrus above low cloud layers. The total cirrus feedback values are not sensitive to the choices of middle/low cloud optical depth and CTP. If the optical depth of middle and low clouds is changed to be 3 or 8 in the kernel calculations, the net cirrus feedback changes only about 5%.

Figure 2.11(a) shows the cloud fraction response to surface temperature anomalies, which is calculated by regressing monthly mean anomalies in cloud fraction against monthly mean anomalies in global mean surface temperature (from ERA-interim). As the surface temperature gets warmer, tropical (30°N-30°S) cirrus cloud fraction increases above and decreases below the altitude at which it peaks on average. This indicates an overall increase in the cirrus altitude in the tropics in agreement with previous studies (Zelinka and Hartmann, 2011) and with theory (Hartmann and Larson 2002). An increase in cirrus fraction is also apparent in over broad range of the mid-latitude upper troposphere of both hemispheres, with no apparent compensatory decreases at other altitudes. The cirrus cloud fraction decreases in polar regions of both hemispheres. Figure 2.11(b) shows the relative humidity response to surface temperature anomalies. The relative humidity response has the same pattern as the cloud fraction response.

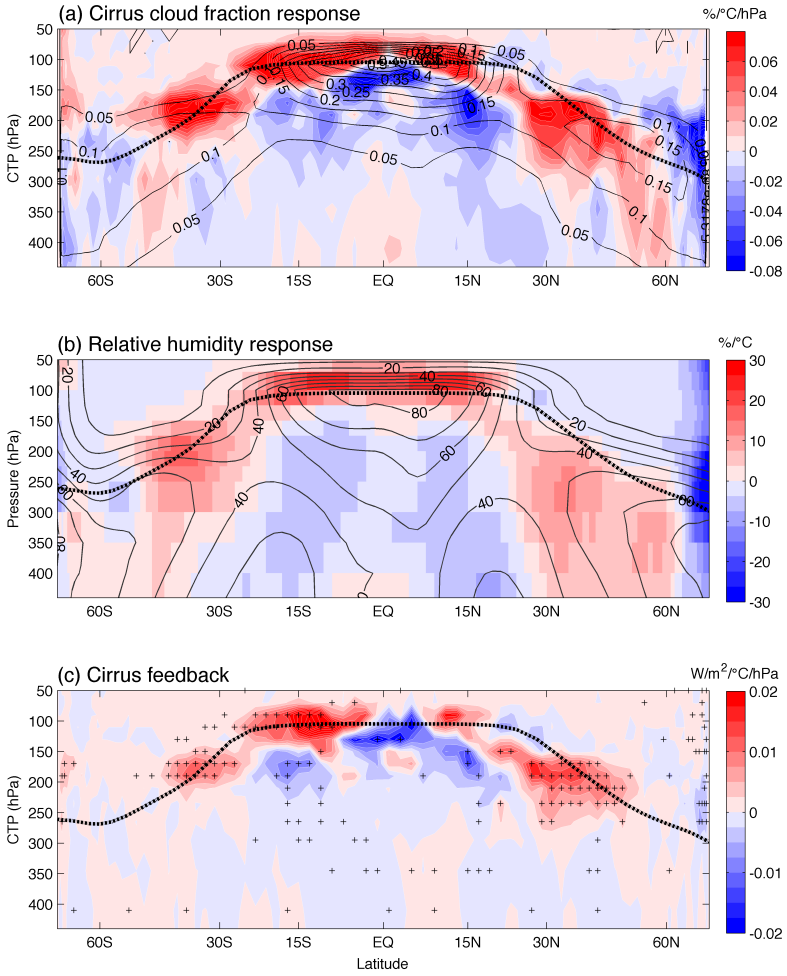

Figure 2.11 Cirrus feedback as a function of latitude and CTP. (a) Response of cirrus clouds fraction to surface temperature anomaly (shading), and the 5-year mean cirrus cloud fraction (in %/hPa, contours). The black dashed line denotes the ERA-interim climatological tropopause. (b) Response of relative humidity to surface temperature anomaly (shading), and the 5-year mean relative humidity (in %, contours). (c) Cirrus feedback as a function of latitude and CTP. Crosses denote pixels where the linear regression is statistically significant.

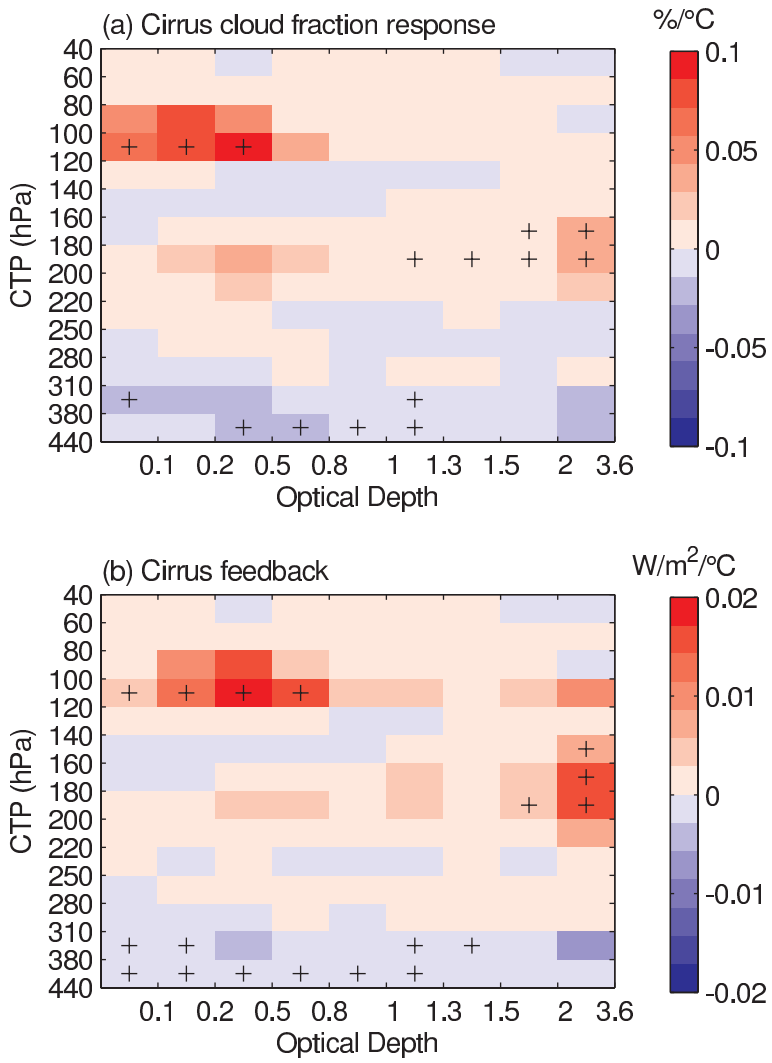

Figure 2.12 Cirrus feedback as a function of CTP and optical depth.

Figure 2.11(c) shows the net cirrus feedback contributed from each latitude-CTP bin. Pixels with positive cirrus fraction response contribute a positive feedback to the climate, and pixels with negative cirrus fraction response contribute a negative feedback. This is because cirrus clouds generally have a warming effect to our climate system. Integrating globally, the short-term net cirrus feedback is estimated to be 0.23±0.22 $W/m^2/°C$, of which the SW component is -0.09±0.28 $W/m^2/°C$ and the LW component is 0.30±0.54 $W/m^2/°C$. This cirrus feedback has a magnitude comparable to short-term and long-term net cloud feedback and surface albedo feedback (Dessler, 2010; Dessler, 2013). Therefore, it is important to the entire climate sensitivity.

The sum of all feedbacks is often referred to as the thermal damping rate; the climate sensitivity is related to the reciprocal of thermal damping rate. Calculations from observations estimate the short-term thermal damping rate to be about -1.15 $W/m^2/°C$ (Dessler 2013). Without the cirrus feedback, the value would be -1.38 $W/m^2/°C$. Therefore, one interpretation of our results is that the cirrus feedback may increases the climate sensitivity calculated from inter-annual climate fluctuations by about 20% in relative to a hypothetical climate state with fixed cirrus clouds.

Figure 2.12 shows the CTP-τ histogram of cirrus feedback. Thin clouds ($\tau<1$) in the tropical tropopause layer (TTL, 80-140 hPa between 30°S and 30°N, Fueglistaler et al.) contribute 0.1±0.08 $W/m^2/°C$, about half of the total cirrus feedback, as a result of the increasing tropical cloud height. TTL cirrus contribute 0.12±0.14 $W/m^2/°C$ to the total cirrus feedback in total, and play an important role in short-term climate fluctuations. The feedback from tropical (30°S-30°N) cirrus is slightly negative, primarily due to a

decrease in tropical cirrus fraction (consistent with Figure10 in Zelinka and Hartmann, 2011), but that is more than made up by changes in mid-latitude cirrus. As a result, the global cirrus feedback is positive.

Cirrus clouds over middle and low clouds play an important role in the short-term feedbacks. For CALIPSO cloud layer product at 1-km resolution, about 9% of the earth's surface is covered by cirrus cloud layers with no other clouds below and about 10% of earth's surface is covered by cirrus overlying middle or low clouds. These cirrus layers above middle or low clouds contribute a feedback of 0.1 $W/m^2/°C$ to the short-term climate, which accounts for about half of the total cirrus feedback.

The positive cirrus feedback could help explain the discrepancy between the short-term cloud feedback calculated from MODIS and that calculated from CERES (Dessler 2010). MODIS often fails to retrieve the cloud properties of thin clouds (Pincus et al. 2012). MODIS detects cirrus in only about 4.5% of the observations (compared to 9% cirrus over clearsky in CALIPSO data), implying that most thin cirrus clouds are not retrieved by MODIS. Thus, this cirrus feedback is at least partially missed by MODIS. CERES, on the other hand, is a broadband flux measurement, so it is expected to incorporate the radiative effect of all clouds. Therefore, if the cirrus feedback was fully accounted for, the total cloud feedback calculated from MODIS would also likely be positive and closer to the value derived from CERES measurements.

The choice of temperature data set had a large impact on the calculation of the total cloud feedback, so we have checked the sensitivity of our net cirrus feedback to the choice of surface temperature dataset. Using GISTEMP instead of ERA-interim surface

temperature, the net cirrus feedback is 0.20±0.24 W/m^2/°C; using NCDC surface temperature, the result is 0.22±0.28 W/m^2/°C; using HadCRUT4, the result is 0.24±0.28 W/m^2/°C. Thus, the uncertainty from the choice of surface temperature dataset is small. Uncertainty from the regression slope is the primary source of short-term cirrus cloud feedback, and the cirrus feedback is statistically distinguished from zero only when ERA-interim surface temperature is used.

The positive cirrus feedback supports the conclusion in Section 2.2: there are generally more thin and high clouds in the free atmosphere in response to inter-annual surface warming, generating a positive feedback.

2.4 Calculation of short-term cloud feedback with ISCCP cloud product

Combining results from MODIS and CALIPSO, it is concluded that there are more low clouds in the boundary-layer in response to inter-annual surface warming, contributing a negative cloud feedback; the overall cloud optical depth decreases, contributing a positive cloud feedback; there is an overall increases in cloud top pressure for clouds in the free atmosphere, contributing a positive feedback. To strengthen these results, we also calculated the short-term cloud feedback with ISCCP cloud product (Zhang et al. 2013, Pincus et al. 2012). To compare with CERES, we use the ISCCP CTP-τ joint histograms between 2000 and 2008.

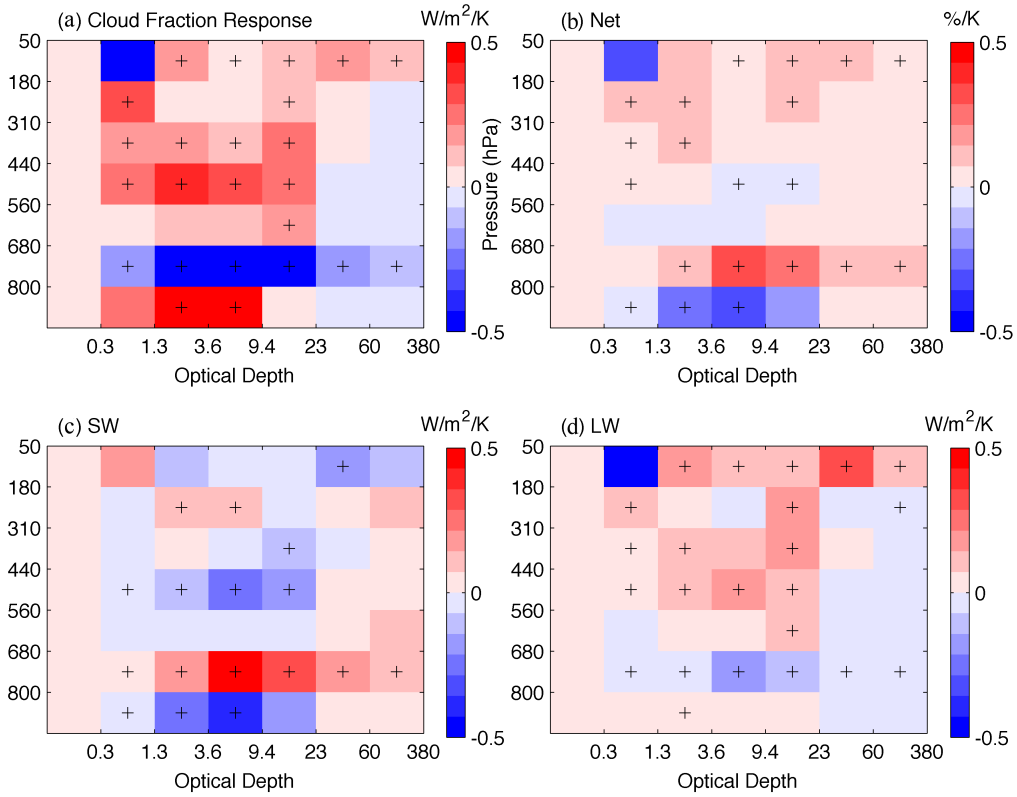

Figure 2.13 Short-term cloud feedback calculated from ISCCP cloud product (2000-2008). (a) Slope of the regression of cloud-fraction anomaly ΔC in each bin vs. ΔT_s (%/K). (b-d) The contribution to the net cloud feedback, SW cloud feedback, and LW cloud feedback, respectively, in W/m^2/K. Note that the multiplication of cloud radiative kernels with cloud fraction anomalies occurs at every location and is then spatially averaged for display in this figure. Bins where the regression slope is statistically significant (>95%) are marked with black crosses.

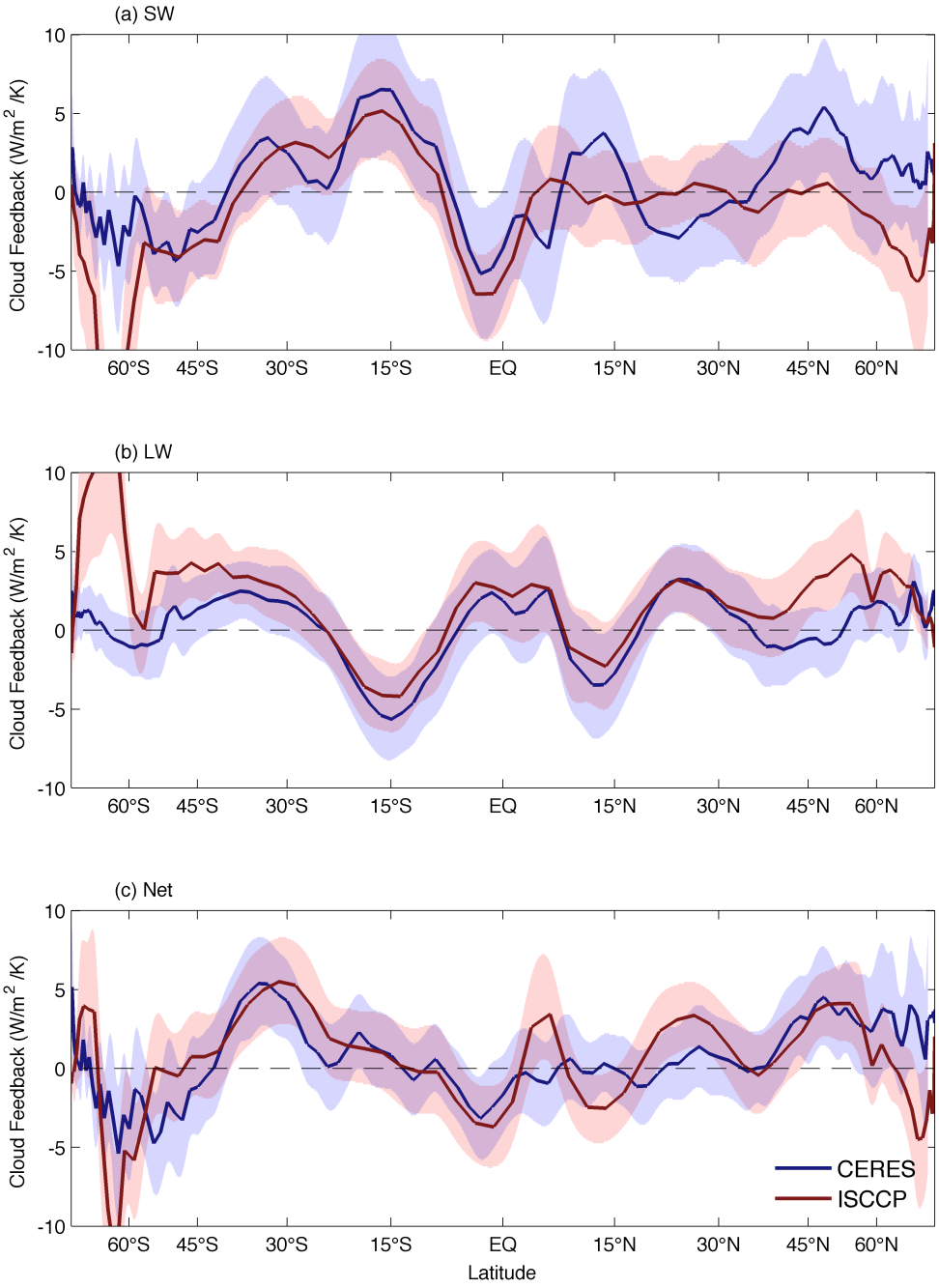

Figure 2.14 The zonal mean cloud feedbacks of ISCCP. The red line is the cloud feedback calculated from ISCCP, and the red shading represents the 95% confidence range. The blue line is the feedback from CERES (Dessler, 2010; 2012), and the blue shading represents the 95% confidence range (where they overlap, the shading is purple).

Figure 2.13(a) shows the slope of the linear regression of global average ΔC vs. ΔT_s in each CTP-τ bin. The results are consistent to MODIS (Figure 2.1). The largest positive slopes (i.e., ΔC increasing with increasing ΔT_s) are found in the lowest height bin (pressures > 800 hPa), with large negative slopes in the bins above (800-680 hPa). Figures 2.13(b), 2.13(c), and 2.13(d) show the net, SW and LW cloud feedbacks, respectively, in each CTP/optical depth bin. There are more high-thin clouds and less low-thick clouds in the free atmosphere (i. e., pressure<800hPa) in response to inter-annual surface warming, contributing a positive feedback; more low clouds in the boundary layer, contributing a negative feedback. The cirrus feedback in ISCCP is also positive, and is consistent to CALIPSO. However, all uncertain clouds are sorted to the $0.3<\tau<1.3$, CTP<180hPa pixel, resulting in an untrue negative cloud amount response in this pixel; there are no clouds in ISCCP histograms with optical depth less than 0.3, and ISCCP may underestimate the cirrus feedback.

However, there is a viewing geometry artifact in the ISCCP data (Evan et al. 2007), so the cloud feedback calculated from ISCCP is less accurate than that calculated from MODIS. Figure 2.14 compares the zonal mean cloud feedbacks calculated from ISCCP and CERES. ISCCP is generally consistent with CERES, but the difference between ISCCP and CERES is much larger than the difference between MODIS and CERES.

2.5 Summation

Observations (MODIS, CALIPSO, ISCCP) suggest that there are more low clouds in the planetary boundary-layer in response to inter-annual surface warming, contributing a negative cloud feedback; the overall cloud optical depth decreases, contributing a

positive cloud feedback; there is an overall increases in cloud top pressure for clouds in the free atmosphere, contributing a positive feedback. The total cloud feedback in response to global surface warming is likely positive, but with large uncertainty.

3. CLOUD RESPONSE TO SURFACE TEMPERATURE TREND AND VARIABILITY IN CLIMATE MODELS

3.1 Model information

Long-term cloud feedback in response to global warming may be different from the cloud feedback in response to inter-annual surface warming. However, decades of observations are needed to determine the long-term cloud feedback, which is not available. In this case, we explore the relationship between short-term and long-term cloud feedback using climate models, and then evaluate the long-term cloud feedback based on observed cloud feedback.

Simulations from the Coupled Model Intercomparison Project Phase 5 (CMIP5, Taylor et al. 2009) are used to search the link between short-term and long-term cloud feedbacks. The Representative Concentration Pathways 6.0 (RCP6) simulations are applied to calculate the short-term cloud feedback in response to climate fluctuations under global warming, and the abrupt $4xCO_2$ experiments are used to calculate the long-term cloud feedback in response to greenhouse gases induced global warming. RCP6 runs are future climate simulations with increasing CO_2 concentration. Abrupt $4xCO_2$ experiments are branched from pre-industrial control runs, and the CO_2 concentration is set to 4 times as much as control runs in the beginning of abrupt $4xCO_2$ experiments.

In this study, 15 models are used to calculate the short-term and long-term cloud feedbacks. They are listed in Table 3.1.

Table 3.1 List of CMIP5 models used in this thesis.

No.	Model Name	Centre	Length of RCP6 runs used (years)	Length of abrupt 4xCO_2 experiments used (years)
1	BCC-CSM1-1	BCC	95	150
2	CCSM4	NCAR	95	151
3	CESM1-CAM5	NCAR	95	150
4	CSIRO-MK3-6-0	CSIRO/ QCCCE	95	150
5	GFDL-CM3	GFDL	95	150
6	GFDL-ESM2G	GFDL	95	300
7	GFDL-ESM2M	GFDL	95	300
8	GISS-E2-H	GISS	95	151
9	GISS-E2-R	GISS	95	151
10	HadGEM2-ES	MOHC	94	151
11	IPSL-CM5A-LR	IPSL	95	260
12	IPSL-CM5A-MR	IPSL	95	140
13	MIROC5	MIROC	95	151
14	MRI-CGCM3	MRI	95	150
15	NorESM1-M	NCC	95	150

3.2 Cloud responses to tropical surface temperature trend and variability

There are two categories of surface temperature changes. The first category is internal surface temperature variability driven by oceanic oscillations, such as ENSO and multi-decadal oscillations. The second category is external climate changes induced by atmospheric radiative forcing, such as global warming. Following Dessler (2013), the cloud feedback in response to short-term internal surface temperature variability is called "short-term cloud feedback" in this study, and the cloud feedback in response to greenhouse gases induced global warming is called "long-term cloud feedback". The measured cloud feedback in Section 2 is a mixture of short-term and long-term cloud feedback, where short-term cloud feedback dominates. In this section, the short-term response of a variable is calculated by regressing the de-trended monthly anomalies of the variable against the de-trended monthly anomalies of surface temperature in RCP6.0 runs. The "obs-like" responses are calculated by regressing the monthly anomalies of the variable against the monthly anomalies of surface temperature in 10-years period of RCP6.0 runs, consistent to the situation of 10 years observation of CERES/MODIS. To be consistent with previous studies, the long-term response of a variable is calculated by regressing the monthly anomalies of the variable against the monthly anomalies of surface temperature in abrupt $4xCO_2$ experiments, which approximately equals to the long-term trend of the variable divided by the long-term trend of surface temperature.

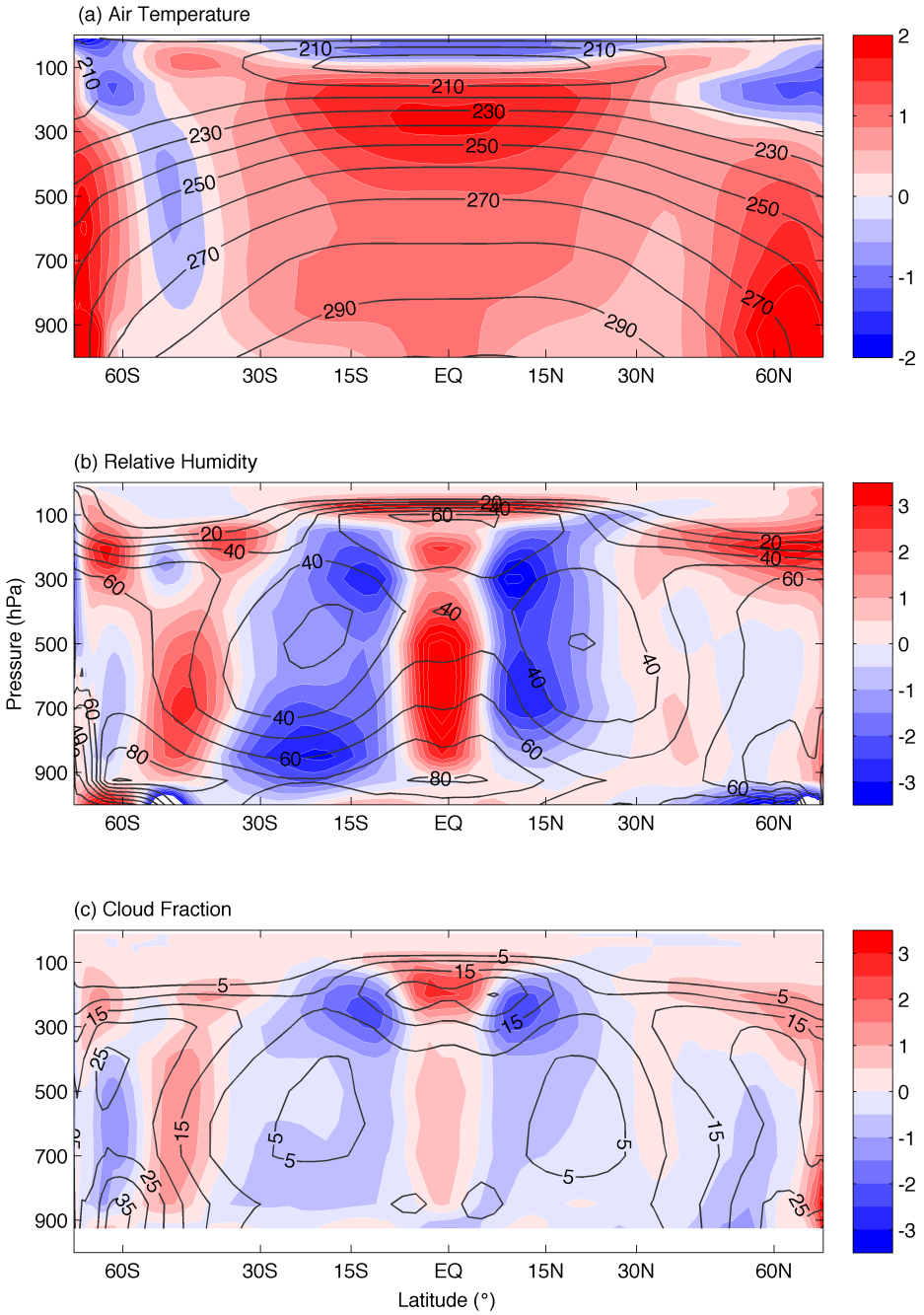

Figure 3.1 Short-term responses in CMIP5 simulations. (a) Air temperature response to the short-term surface temperature variability in CMIP5 simulations (ensemble average). Contours are climatological values. (b) Relative humidity response. (c) Cloud fraction response.

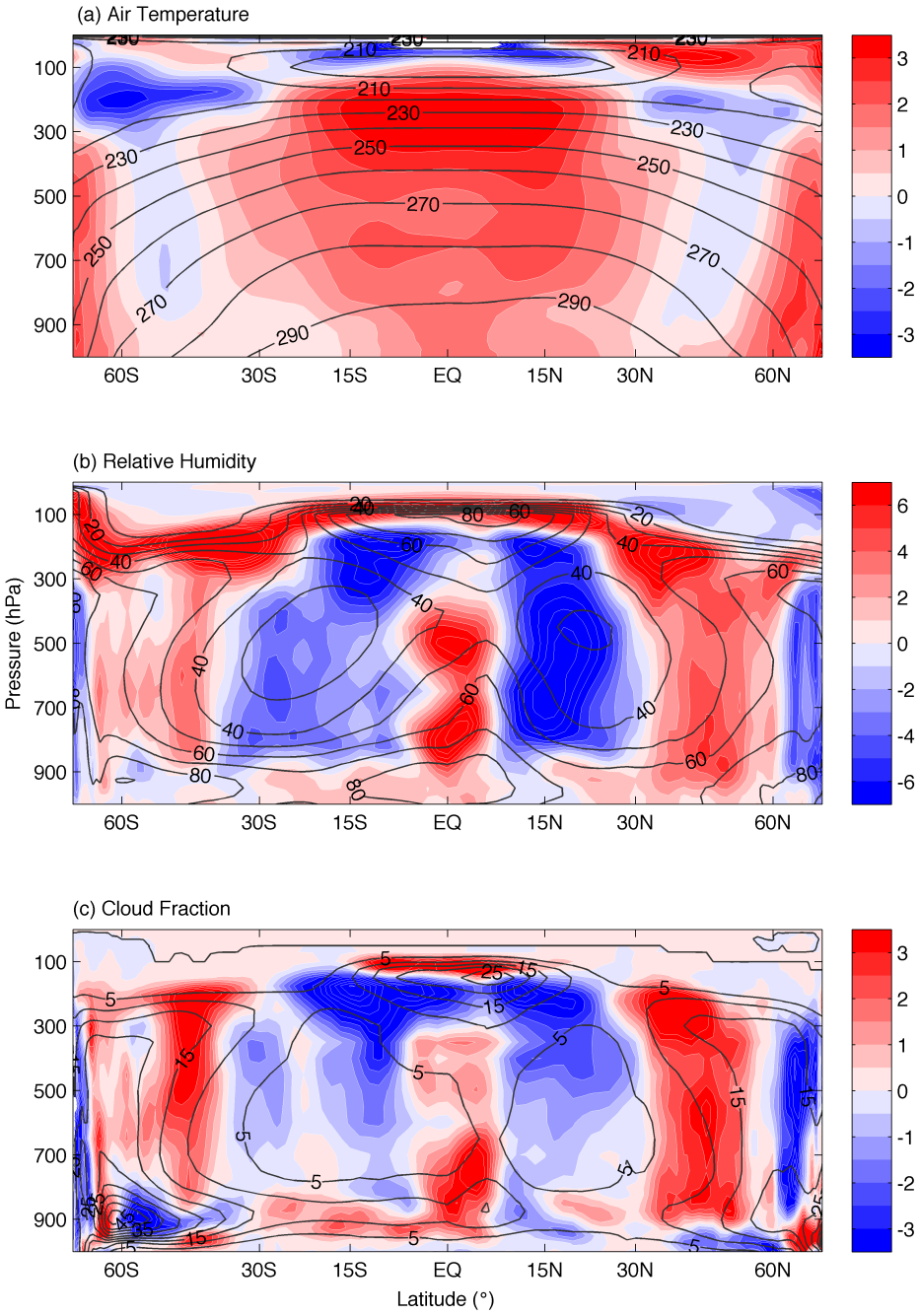

Figure 3.2 Short-term responses calculated from observations and reanalysis. (a) Air temperature response to the short-term surface temperature variability in ERA-interim. Contours are climatological values. (b) Relative humidity response. (c) Cloud fraction response.

Figure 3.1(a) shows the air temperature response to the surface temperature variability in CMIP5 simulations, which is calculated by regressing the de-trended air temperature anomaly against the de-trended surface temperature anomaly. El Nino is the most significant event in inter-annual timescale, and the inter-annual surface warming concentrates in the deep tropics. The specific humidity near the tropical sea surface increases in response to surface temperature warming, and thus there is more liquefied water vapor in the tropical troposphere, releasing more latent heat. Therefore, there is an enhanced warming in the tropical troposphere (Santer et al. 2005). Figure 3.1(b) shows the relative humidity response to surface temperature variability. In the troposphere, the relative humidity increases in the deep tropics and mid-latitudes, and decreases in the subtropics, primarily due to an strengthened and narrowed Hadley Circulation. Near the tropopause and in the lower stratosphere, the relative humidity increases. Figure 3.1(c) shows the response of cloud fraction to surface temperature variability. The zonal mean cloud fraction response has the same pattern as the relative humidity pattern, consistent to the cirrus cloud fraction response in Section 2.

Figure 3.2(a) shows the air temperature response to the surface temperature variability calculated from ERA-interim, 2006-2013. The pattern of air temperature response to the surface temperature variability is same in the simulations and the reanalysis, implying that the models are doing well in simulating the short-term temperature response. The amplitude of low tropospheric warming in the tropics is different in the models and reanalysis, probably due to difference in El Nino strength. Figure 3.2(b) shows the relative humidity response to surface temperature variability

calculated from ERA-interim, and Figure 3.2(c) shows the cloud fraction response calculate from CloudSat observations. CMIP5 and observations show similar patterns in temperature, relative humidity and cloud fraction response, implying that the GCMs are doing well in simulating water vapor and cloud changes in the free atmosphere. However, the response of low clouds is inconsistent in GCMs and observations. Observations suggest that the low cloud fraction increases in response to surface temperature variability, but in models the low cloud fraction decreases. This difference would result in overestimation of short-term cloud feedback.

Figure 3.3 shows the temperature, relative humidity and cloud fraction responses to long-term global warming. The relative humidity and cloud responses to long-term surface warming have different patterns from the response to inter-annual surface temperature variability. The reason is that the circulation response to the inter-annual surface temperature variability and long-term surface warming are different, and therefore the latitude distribution of cloud fraction response to surface temperature trend is different from the short-term response. Figures 3.4-3.7 illustrate the relationship between circulation response and cloud fraction response to surface air temperature trend and variability.

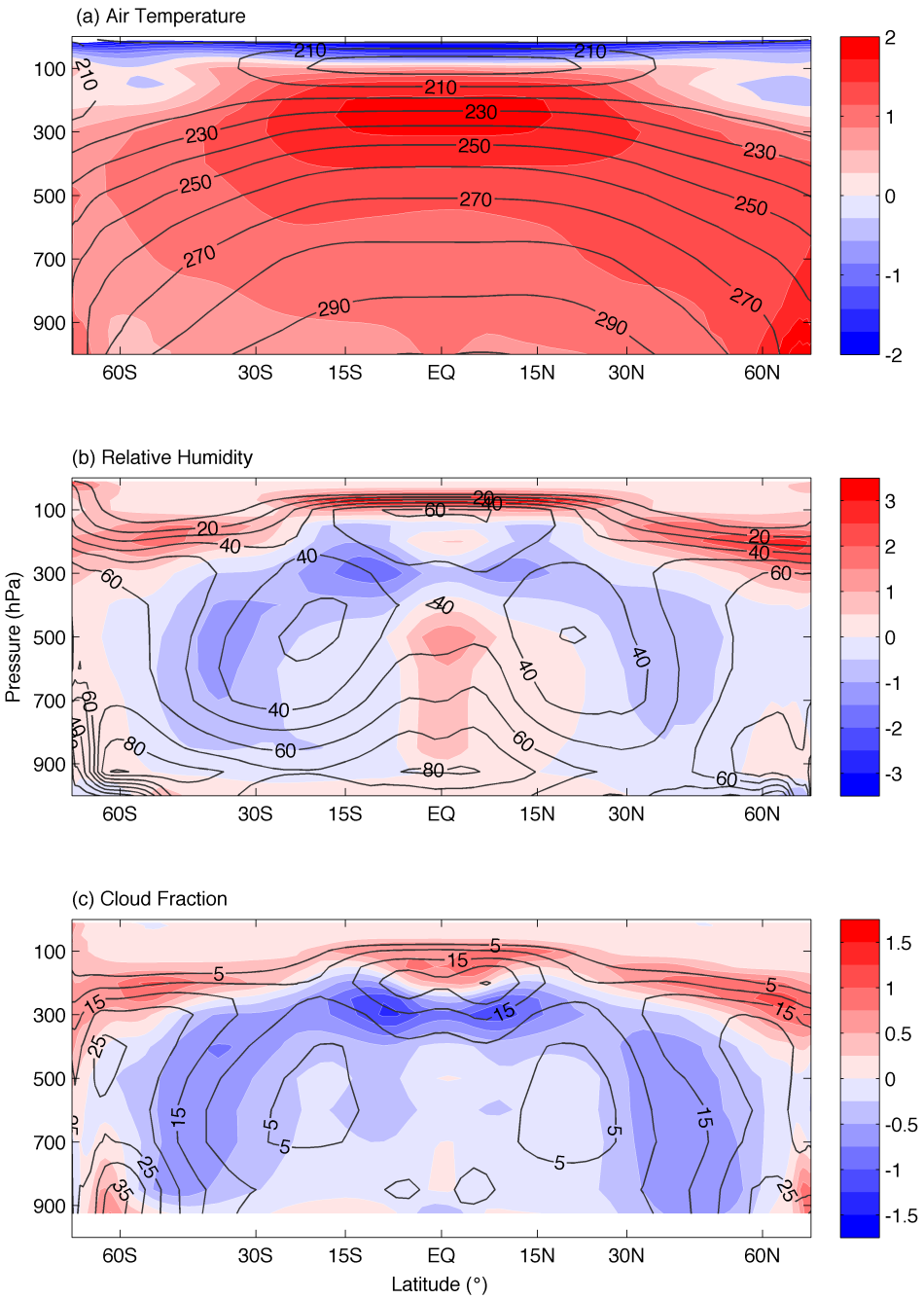

Figure 3.3 Long-term responses in CMIP5 simulations. (a) Air temperature response to the long-term surface warming. Contours are climatological values. (b) Relative humidity response. (c) Cloud fraction response.

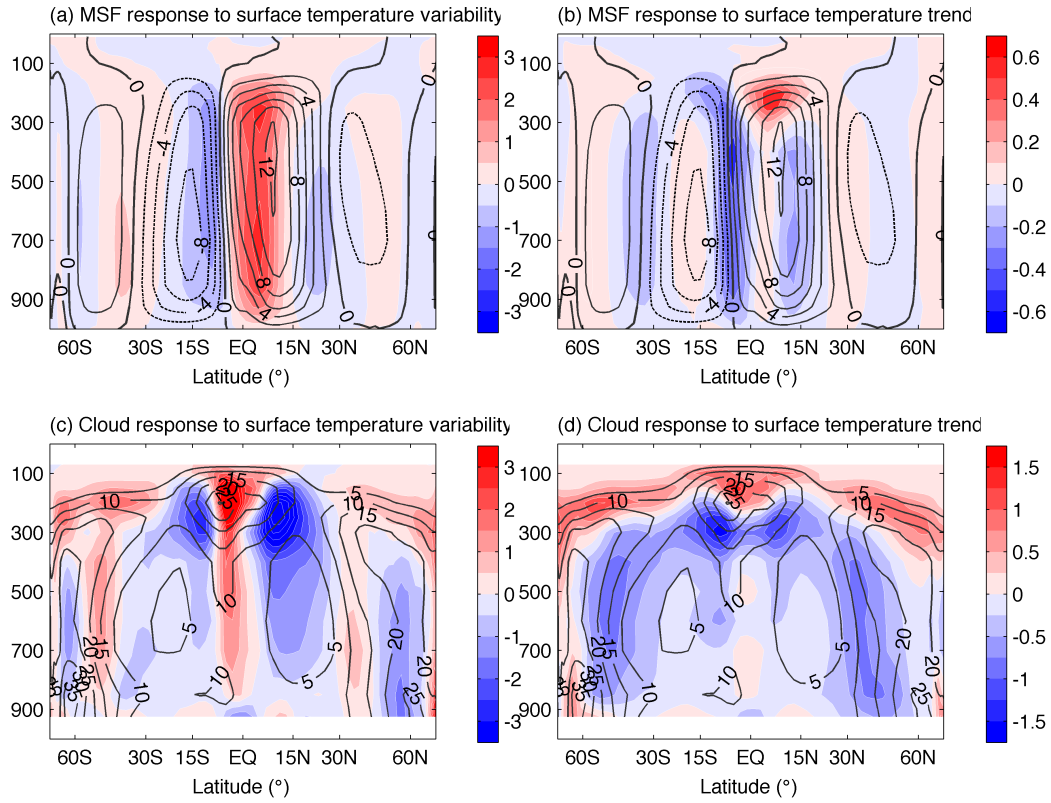

Figure 3.4 Circulation and cloud response in CMIP5 simulations in March, April and May. (a) Response of MSF to inter-annual. The contours are climatological values, and the unit is 10^{10}kg/s. (b) Response of MSF to long-term global warming. (c) Response of cloud fraction to inter-annual variability. Contours are climatological values, and the unit is %. (d) Response of cloud fraction to long-term global warming.

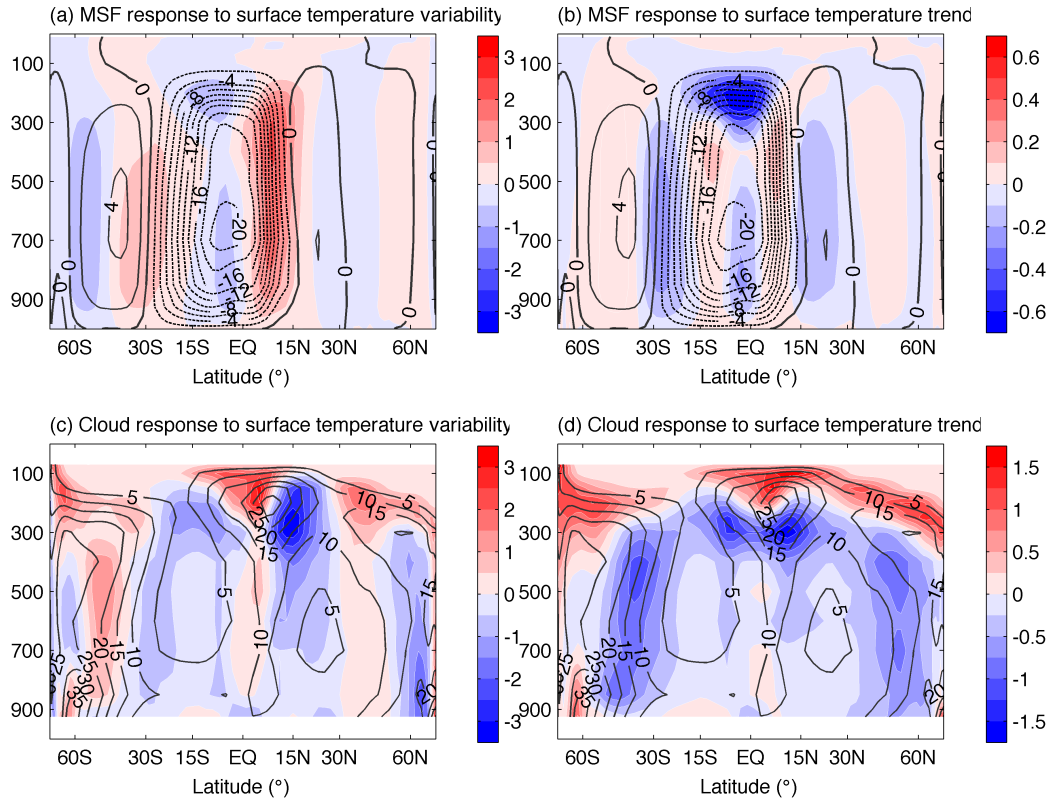

Figure 3.5 Circulation and cloud response in CMIP5 simulations in June, July and August.

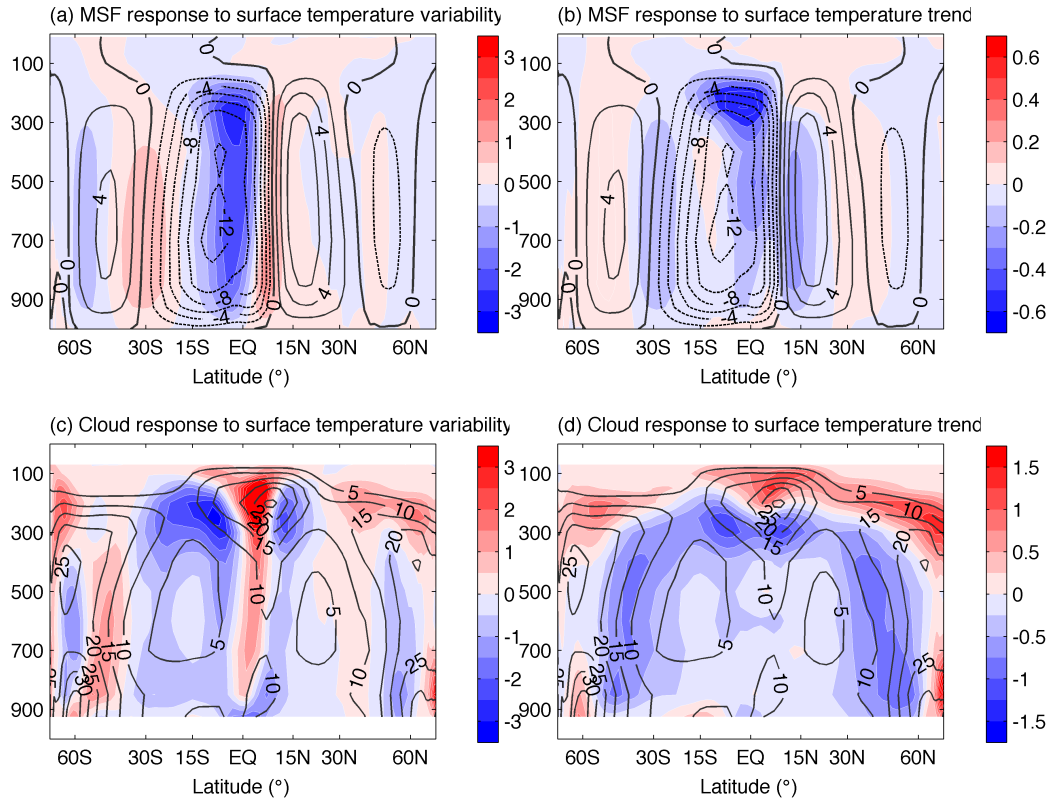

Figure 3.6 Circulation and cloud response in CMIP5 simulations in September, October, and November.

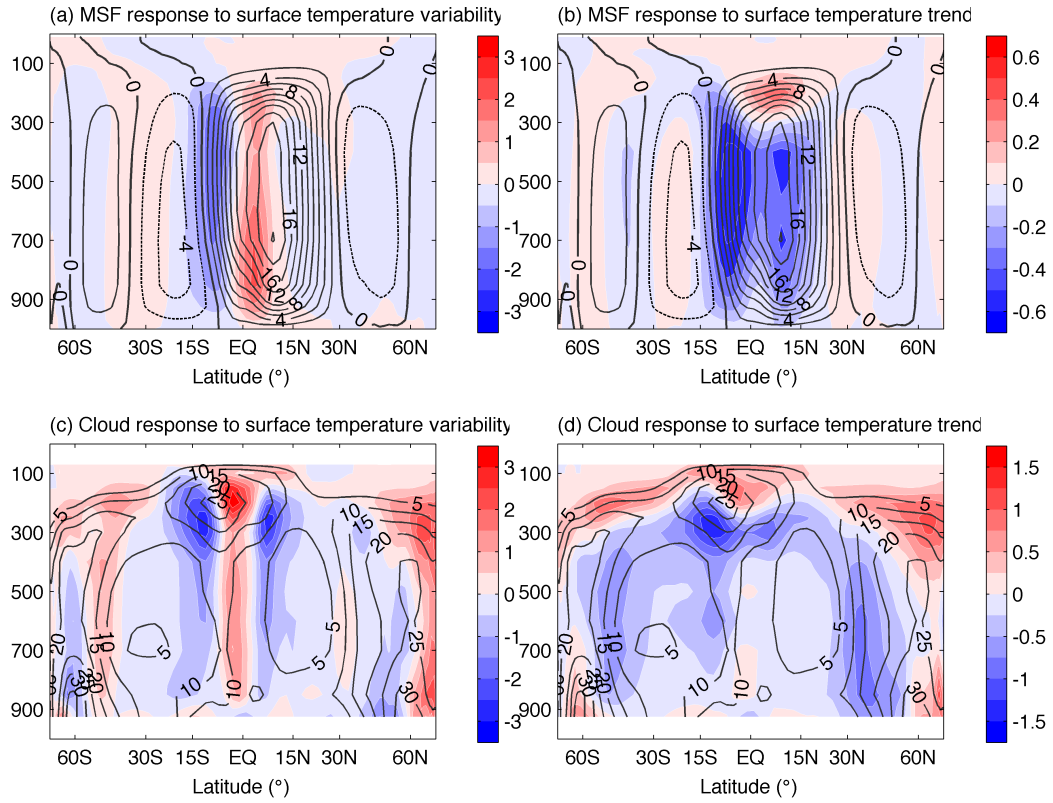

Figure 3.7 Circulation and cloud response in CMIP5 simulations in December, January and February.

Contours in Figures 3.4(a) are climatological meridional mass stream function (MSF) averaged over March, April and May. The MSF is defined as (Holton 1994):

$$\psi(lat,p)=\frac{2\pi a\cos(lat)}{g}\int_0^p[v(lat,p)]dp\,, \tag{3.1}$$

where a is earth's radius, p is pressure, g is gravity, and [v] is zonal mean meridianal wind velocity. The MSF contours denote meridional circulations:

$$[v]=\frac{g}{2\pi a\cos(lat)}\frac{\partial\psi}{\partial p}\text{, and} \tag{3.2}$$

$$[w]=-\frac{g}{2\pi a^2\cos(lat)}\frac{\partial\psi}{\partial(lat)}\,. \tag{3.3}$$

Between the Equator and 30°N, the MSF is positive with a maximum at 500hPa, indicating that there is a clockwise meridional circulation in the Northern Hemisphere (NH) tropics, which is called the Hadley Circulation (Holton 1994). The maximum value denotes the strength of Hadley Circulation. The tropospheric MSF is negative between 30°N and 60°N, indicating an anti-clockwise circulation named Ferrel Circulation. In the Southern Hemisphere (SH), the direction of Hadley Circulation and Ferrel Circulation are opposite to the Northern Hemisphere, so the MSF is negative in the SH tropics, and positive in the SH mid-latitudes. The MSF between 15°N and Equator increases in response to inter-annual surface warming, and the MSF between 15°S and Equator decreases in response to inter-annual surface warming, indicating that the Hadley Circulations are intensified. The MSF decreases at the NH Hadley Circulation boundary (around 30°N) and increases at the SH Hadley Circulation boundary (around 30°S), indicating that the Hadley Circulations are narrowed in response to inter-annual surface

warming. Correspondingly, the tropical clouds concentrates into the deep tropics, so the cloud fraction increases in the deep tropics and decreases around 15°S and 15°N (Figure 3.4c). On the upper branch of Hadley Circulations (around 200hPa), the MSF increases in NH tropics and decreases in SH tropics, implying that the Hadley circulation is developing deeper in response to inter-annual surface warming. Correspondingly, the overall cloud height also increases in response to inter-annual surface warming.

The circulation change in response to long-term global warming is different from the inter-annual surface warming. The maximum MSF value of the NH tropics decreases, and the minimum MSF value in the SH tropics increases, indicating that the Hadley Circulations are weakened in response to global warming. The MSF increases at the NH Hadley Circulation boundary (around 30°N) and decreases at the SH Hadley Circulation boundary (around 30°S), indicating that the Hadley Circulations are widening in response to long-term global warming (Hu and Fu 2007, Lu et al. 2008, Hu et al. 2011). As a result, the latitudinal distribution of cloud response in Figure 3.4(d) is different to that in Figure 3.4(c). On the other hand, the Hadley Circulations also develop deeper in response to global warming, so the overall cloud height also increases in response to inter-annual surface warming.

Figures 3.5-3.7 show the responses of MSF and cloud fraction in the other three seasons. In all the seasons, the Hadley Circulations develops deeper in response to inter-annual surface warming and long-term global warming, resulting in an increase in the overall cloud height.

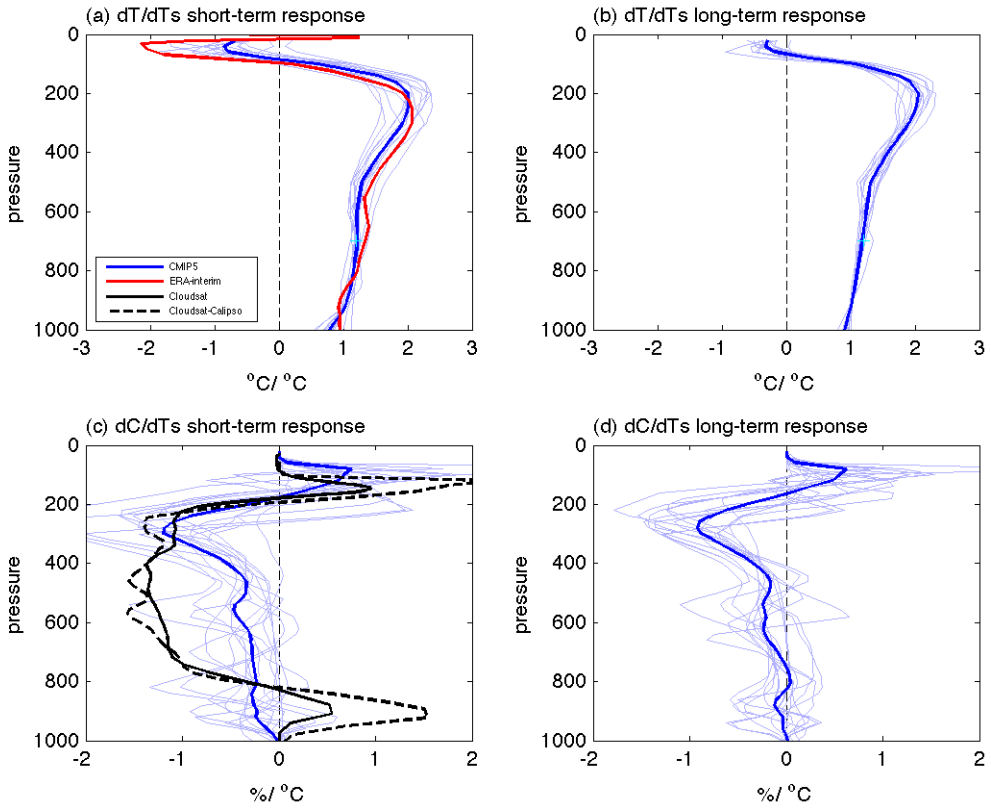

Figure 3.8 Vertical profiles in the tropics. (a) Tropical air temperature response to the short-term surface temperature variability in CMIP5 simulations (blue), and ERA-interim (red). (b) Air temperature response to long-term surface temperature trend in CMIP5 4xco2 simulations. (c) Cloud fraction responses to short-term surface temperature variability in pressure levels. Blue lines are CMIP5 simulations, black solid line is calculated from Cloudsat level-2B CPR cloud mask data, and black dashed line is calculated from Cloudsat level-2B cloud CPR+CALIPSO Lidar cloud mask data (2006-2010). (d) Cloud fraction responses to long-term surface temperature trend in CMIP5 4xCO_2 simulations.

Bony et al. (2004) found that the tropically averaged cloud radiative effect was mainly controlled by thermodynamic changes of tropical atmosphere, and dynamic changes only affect local cloud radiative effect. Therefore, we search for the link between short-term and long-term cloud feedback by analyzing tropical averages.

In order to investigate the connection between short-term and long-term cloud feedbacks in the tropics, we explored the cloud response to tropical (30°S-30°N) surface temperature trend and variability with CMIP5 simulations. Figure 3.8(a) shows the short-term tropical air temperature response to surface temperature variability in CMIP5 RCP6 simulations, which is calculated as the regression slope of de-trended tropical air temperature monthly anomaly against the de-trended tropical surface temperature monthly anomalies. The tropical surface warming is amplified in the troposphere (Santer et al. 2005), with a maximum at about 250hPa. The stratospheric air temperature decreases as atmospheric carbon dioxide increases. Results from ERA-interim (1979-2013) are also plotted in Figure 3.8(a), and are consistent with CMIP5 simulations. Figure 3.8(b) shows the long-term air temperature response to a surface temperature trend in tropical area, which is calculated from CMIP5 4xCO_2 experiments. The long-term tropical air temperature response to surface temperature trends has the same profile as the short-term response, implying that the thermodynamic changes in the tropics are the same in response to tropical surface temperature trend and variability.

Figure 3.8(c) shows the short-term tropical cloud fraction response to surface temperature variability in CMIP5 RCP6.0 simulations. There is a decrease in middle and low clouds and an increase in the highest clouds in response to surface warming, which

generates a positive tropical cloud feedback (Zelinka et al. 2011). We also plot the cloud fraction response from Cloudsat level-2 data. Observations show a much larger decrease in cloud fraction between 300hPa and 800hPa, combined with an increase in the highest level of clouds. Both observations and CMIP5 simulations suggest that clouds in the free atmosphere get higher in response to inter-annual surface warming.

However, results from Cloudsat show that low clouds in the PBL (typically P > 800 hPa) increase in response to inter-annual surface warming in the tropics, which are different from CMIP5 simulations, but are consistent to MODIS observations. Figure 3.8(d) shows the long-term tropical cloud fraction response to long-term surface temperature trends in CMIP5 RCP6.0 simulations. Cloud fraction response to tropical surface temperature trend and variability is similar in climate models.

3.4 Link between short-term and long-term cloud feedbacks

Uncertainty on PBL clouds in GCMs is the primary source of the large spread in GCM predicted cloud feedbacks (Bony et al. 2005). Figure 3.9(a) shows the relationship between tropical cloud feedbacks and the PBL cloud fraction responses (averaged between 800-1000 hPa pressure levels) to tropical surface temperature changes. Tropical cloud feedbacks, both short-term and long-term, are well correlated with PBL cloud fraction responses. MODIS and CERES observations fall at the low-sensitivity end of the line — mainly because the observations show that PBL cloud fraction increases in response to surface temperature variability, but most models show that PBL cloud fraction decreases in response to surface temperature trend and variability.

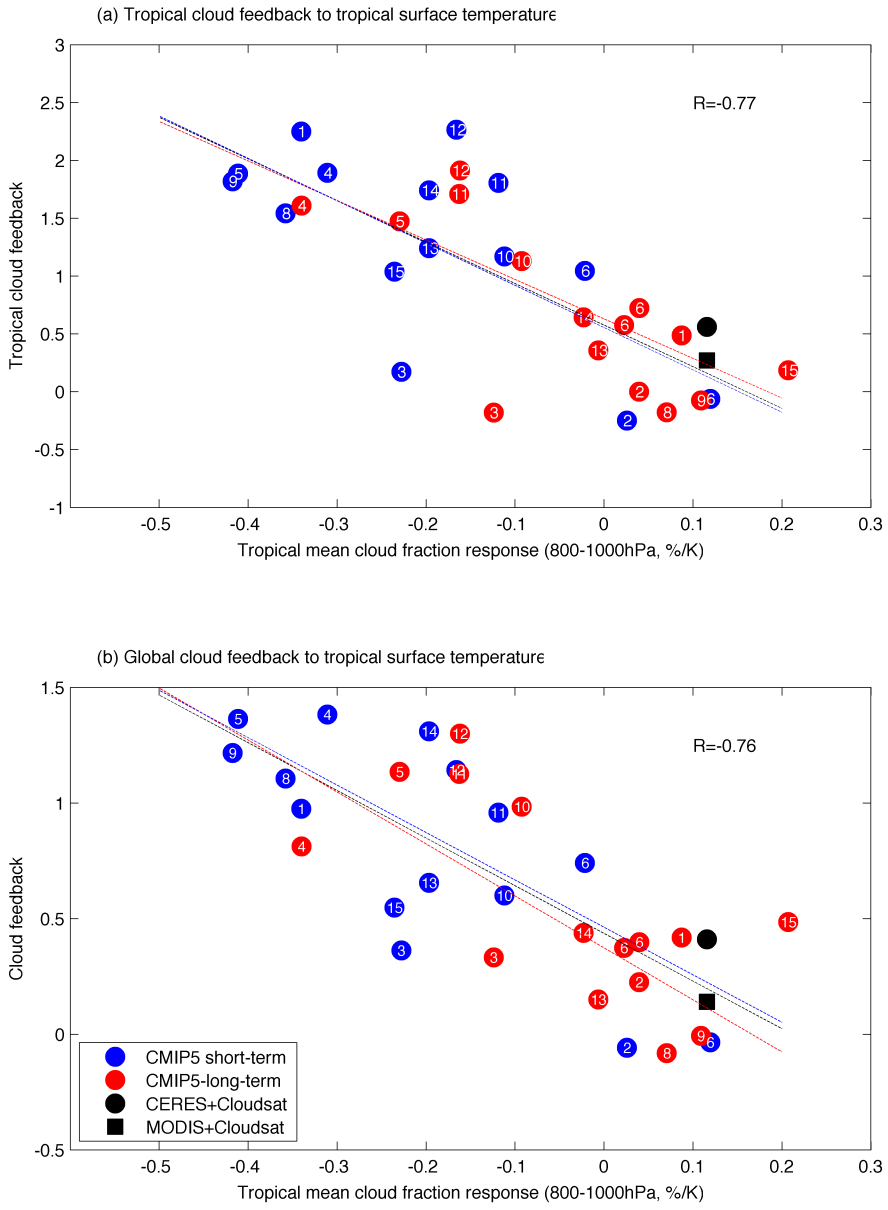

Figure 3.9 Link between short-term and long-term cloud feedback. (a) Tropical cloud feedback as a function of tropical PBL cloud fraction response (800-1000hPa). The Blue points are calculated from short-term climate fluctuations, and red points are calculated from long-term changes. The black point is plotted using cloud feedback from CERES (Dessler 2010) and Cloudsat cloud fraction. The black square is plotted using cloud feedback from MODIS and Cloudsat cloud fraction. The black line is least square fit line of CMIP5 models (both short-term and long-term feedback). (b) Global cloud feedback in response to tropical surface temperature changes.

Figure 3.9(b) shows the relationship between the global cloud feedback in response to tropical surface temperature changes and the PBL cloud fraction responses. This global cloud feedback is also well correlated with PBL cloud fraction responses. Therefore, the cloud feedback in response to short-term tropical surface temperature fluctuations and long-term tropical surface temperature trends does not only follow the same mechanism, but also has same magnitude if the PBL cloud response is given.

Therefore, it is reasonable to evaluate the model predicted long-term cloud feedback using observed short-term cloud feedback. If the short-term cloud feedback in climate models is consistent with observations, it is likely that the long-term cloud feedback in models are also correct; if the short-term cloud feedback in models are not consistent with observations, it is likely that the long-term cloud feedback in models are also wrong.

3.5 Summation

Climate models generally show a positive cloud feedback in response to surface temperature trend and variability. In response to surface temperature changes, there is a decrease in the middle/low cloud amount and an increase in high cloud amount, indicating an overall increase in cloud height.

The spatial pattern of short-term cloud response to surface temperature trend is different from the spatial pattern of long-term cloud response to surface temperature variability. However, integrating tropically, the vertical profile is same for short-term and long-term cloud responses to tropical surface temperature trend and variability.

The cloud feedback in response to tropical surface temperature trend and variability has same magnitude if the PBL cloud responses are same. Therefore, the short-term and long-term cloud feedbacks follow the same mechanism in the free atmosphere, and it is reasonable to evaluate long-term cloud feedback using observed short-term cloud feedback.

4. EVALUATION OF LONG-TERM CLOUD FEEDBACK PREDICTED BY GCMS

4.1. Comparison of short-term cloud feedback in models and observations

Figure 4.1 shows the short-term cloud feedback in response to tropical surface temperature changes in 10-year periods. For each model, the RCP6.0 21st century simulation is sorted into nine 10-year periods, and the cloud feedback values are calculated for each period. Unnumbered and colored signs denote values calculated from a 10-year period in each model, and numbered black points are average values for each model. The relationship of Figure 3.5 still holds. In addition, the average low cloud fraction response in nine 10-year periods is close to the short-term response in Figure 3.5.

According to Figure 4.1, the low cloud fraction response has large spread in different 10-year periods for each model. Change of low cloud fraction is different to in response to inter-annual surface warming and long-term global warming, different among climate models, and different among 10-year periods. Most models suggest that the tropical low cloud fraction decreases in response to inter-annual surface warming, and are not consistent with observations.

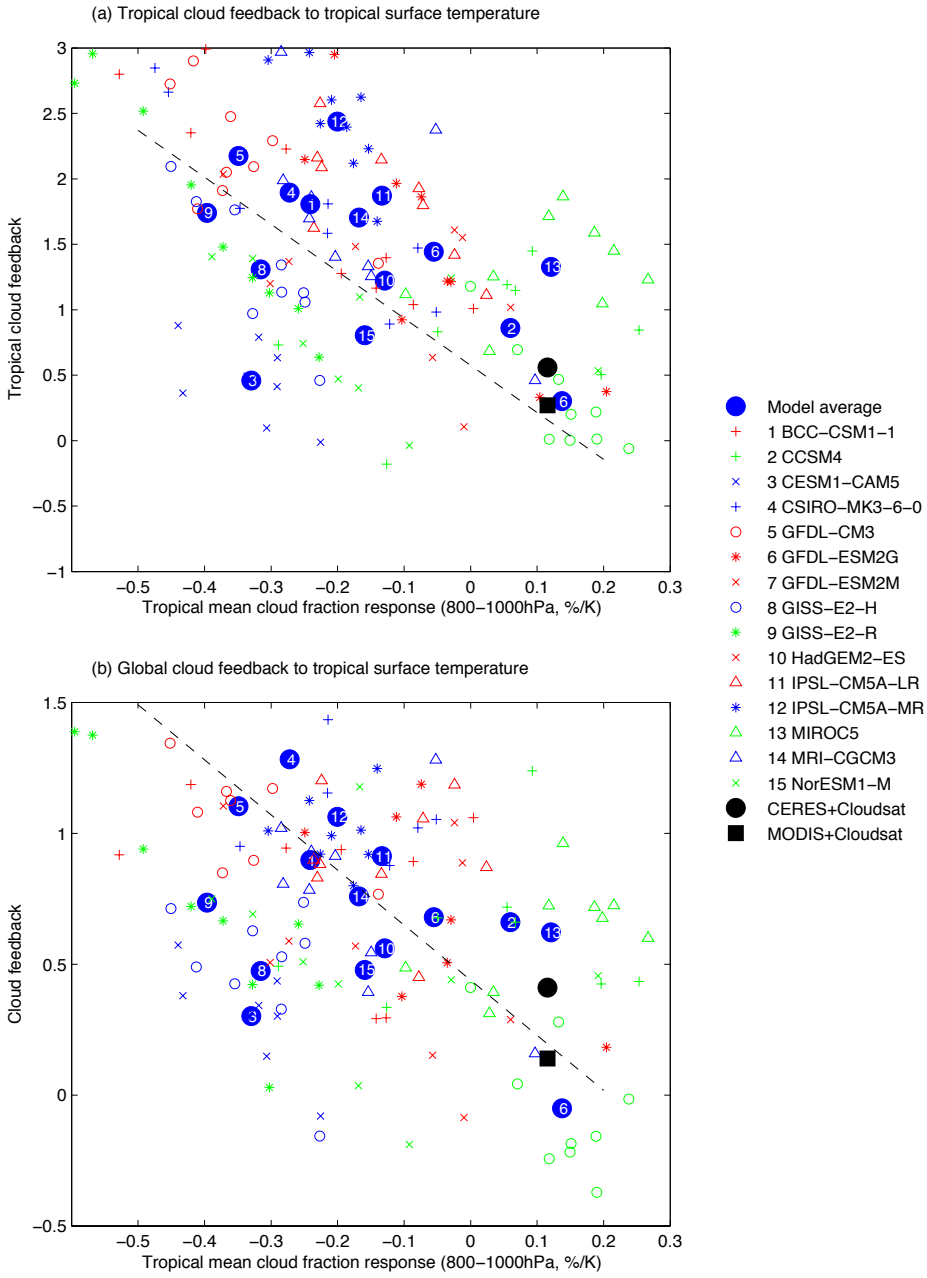

Figure 4.1 Obs-like short-term cloud feedback in CMIP5 simulations. (a) Tropical cloud feedback as a function of tropical PBL cloud fraction response (800-1000hPa). Unnumbered and colored signs denote values calculated from a 10-years period in each model (obs-like), and numbered black points are average values for each model. The black points and black lines are the same as that in Figure 3.5. (b) Global cloud feedback in response to tropical surface temperature changes.

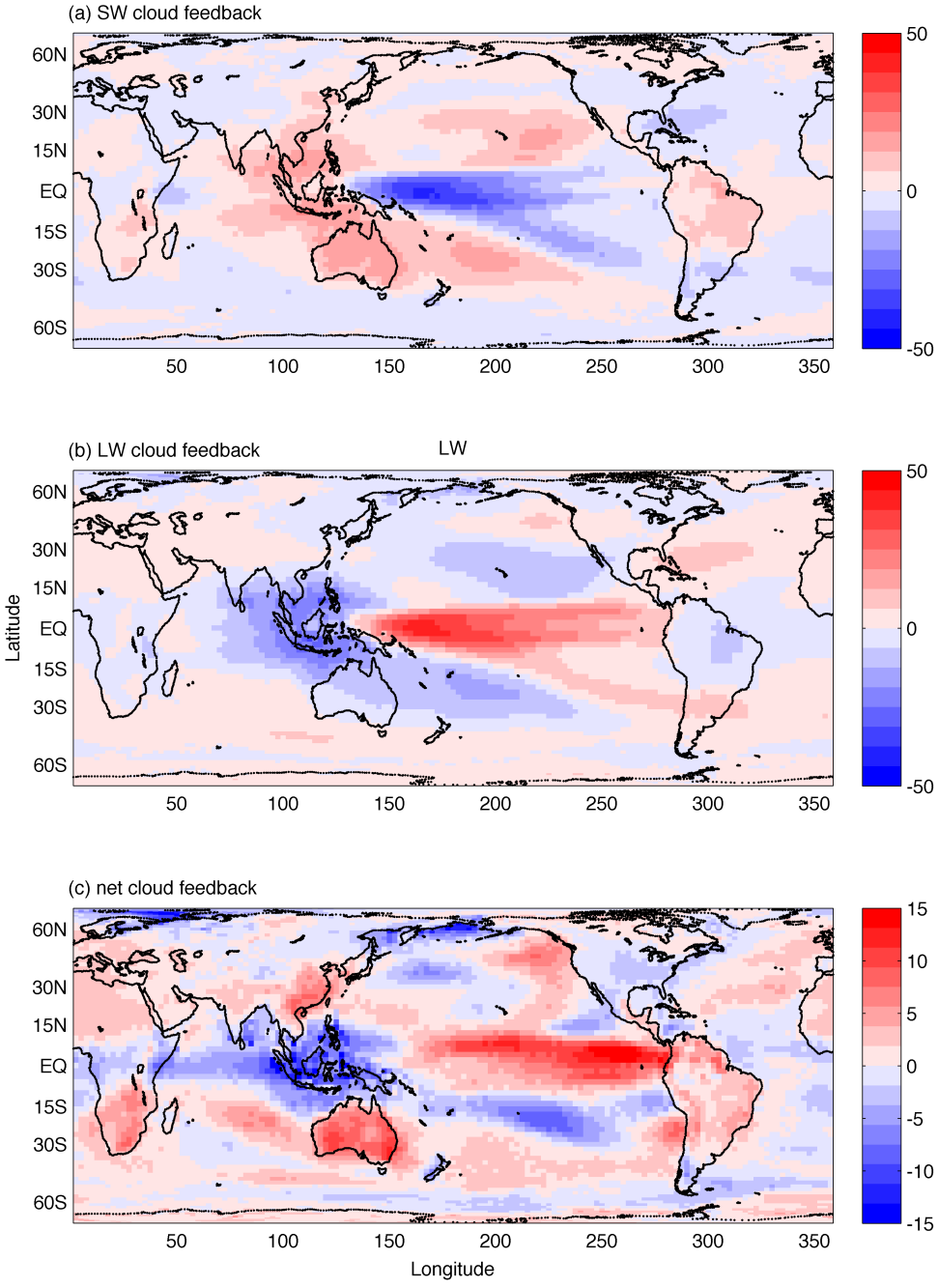

Figure 4.2 Spatial pattern of the 10-year cloud feedback, averaged over all periods and models in CMIP5 RCP6 simulations. The unit is $W/m^2/K$.

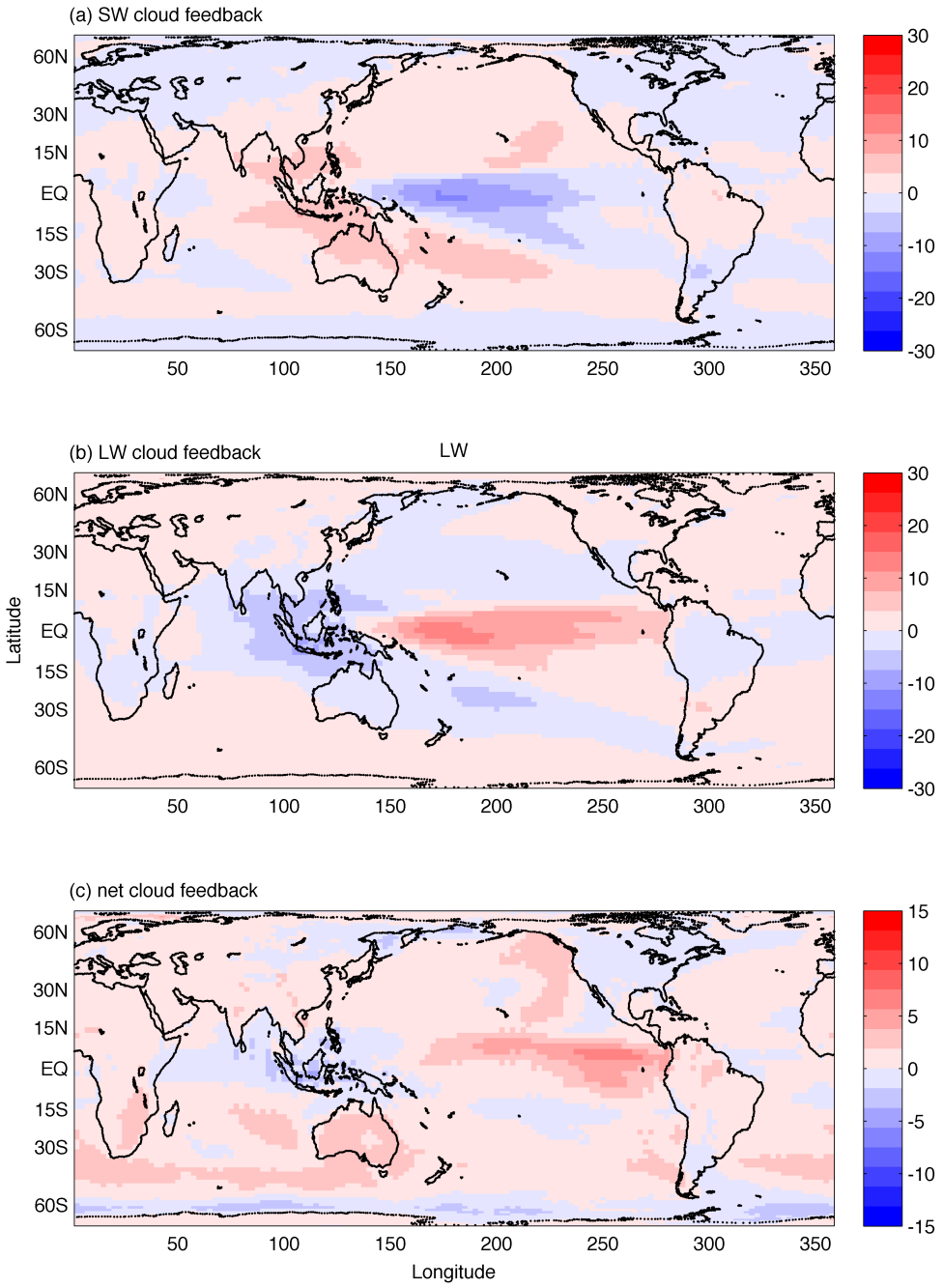

Figure 4.3 Spatial pattern of the long-term cloud feedback, averaged over all models in CMIP5 4xCO_2 simulations. The unit is W/m^2/K.

Figure 4.2 shows the spatial pattern of the SW, LW and net cloud feedbacks in CMIP5 RCP6 10-year periods. The SW and LW cloud feedbacks in climate models are generally consistent with observations (Figure 2.3). However, the net cloud feedback is different in models and observations, implying that the high-thick cloud responses in models may be consistent with observations, so low cloud and cirrus cloud responses may be responsible for differences in regional net cloud feedback. According to Figure 3.8(a), tropical high cloud responses are consistent in models and observations, so it is indicated that the difference in regional net cloud feedback between models and observations are primarily induced by differences in low cloud response.

Long-term cloud feedbacks calculated from CMIP5 4xCO_2 experiments has different spatial pattern from short-term cloud feedbacks (Figure 4.3). Inter-annual surface warming is concentrated in the deep tropics, so the absolute value of regional cloud feedbacks is large; long-term global warming distributes more uniformly on the earth surface, and the long-term cloud feedbacks also distribute more uniformly and have smaller magnitude than short-term cloud feedbacks.

In conclusion, it is likely that the middle and high cloud responses to surface warming in GCMs are correct, but the low cloud response in GCMs is biased.

4.2 Low cloud fraction and EIS

Wood and Bretherton (2006) introduced the estimated inversion strength (EIS), which well explains the variation in stratiform low cloud cover. EIS is calculated from the following equation:

$$EIS = LTS - \Gamma_m(z_{700} - LCL), \tag{4.1}$$

where *LTS* is the lower-tropospheric stability, z_{700} is the height of 700hPa pressure level, *LCL* is the lifting condensation level, and Γ_m is the average moist adiabatic potential temperature gradient between the surface and 700hPa. Γ_m can be calculated as

$$\Gamma_m(T,p) = \frac{g}{c_p}\left(1 - \frac{1 + L_v q_s(T,p)/R_a T}{1 + L_v^2 q_s(T,p)/c_p R_v T^2}\right), \tag{4.2}$$

where g is the gravitational acceleration, c_p is the specific heat of air at constant pressure, L_v is the latent heat of vaporization, q_s is the saturation mixing ratio, R_a is the gas constants for dry air, and R_v is the gas constants for water vapor.

The change of EIS can also be calculated approximately as (Qu et al. 2013)

$$\Delta EIS = 0.97 * \Delta T_{700} - 1.14 \Delta Ts, \tag{4.3}$$

Where ΔT_{700} is the change in the 700hPa air temperature.

Figure 4.4 shows the relationship between tropical mean EIS and low cloud fraction (CTP<680hPa). The EIS is well correlated with the low cloud fraction, and the positive low cloud fraction response is likely induced by positive EIS response to inter-annual surface warming. Most of low clouds are over oceans, and the tropical low cloud fraction anomaly is well correlated to the tropical oceanic low cloud fraction anomaly.

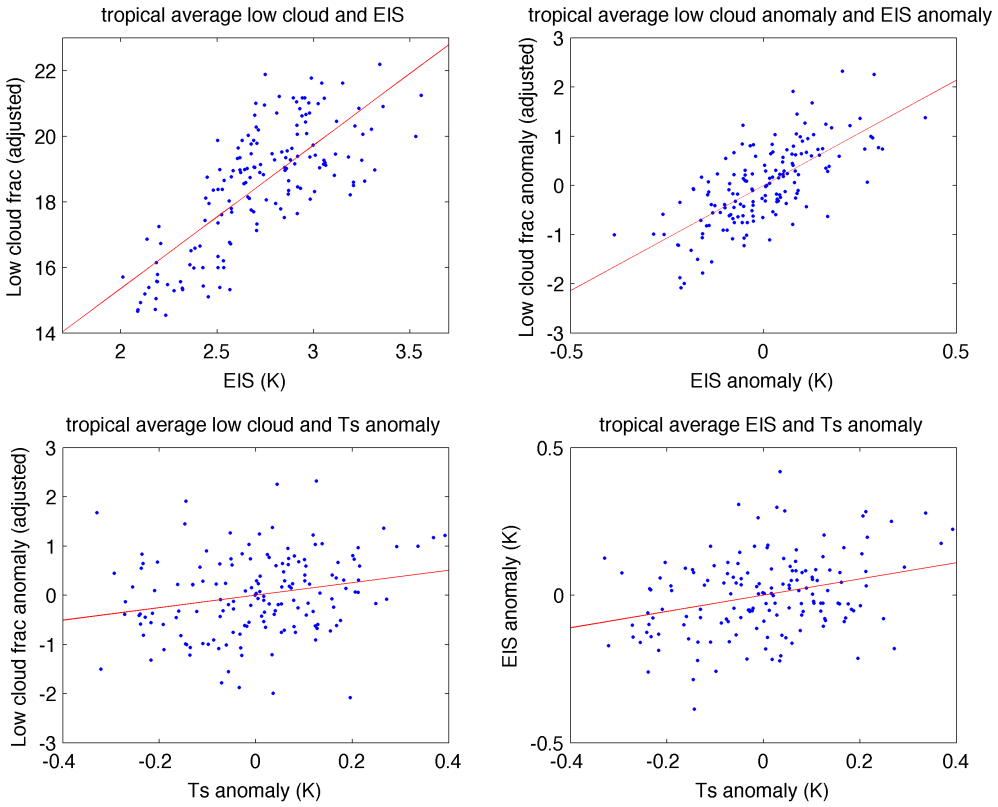

Figure 4.4 Relationship between tropical average EIS and tropical average low cloud fraction (CTP<680hPa). EIS and ΔT_s are calculated from ERA-interim, and low cloud fraction is calculated from MODIS (2000-2012).

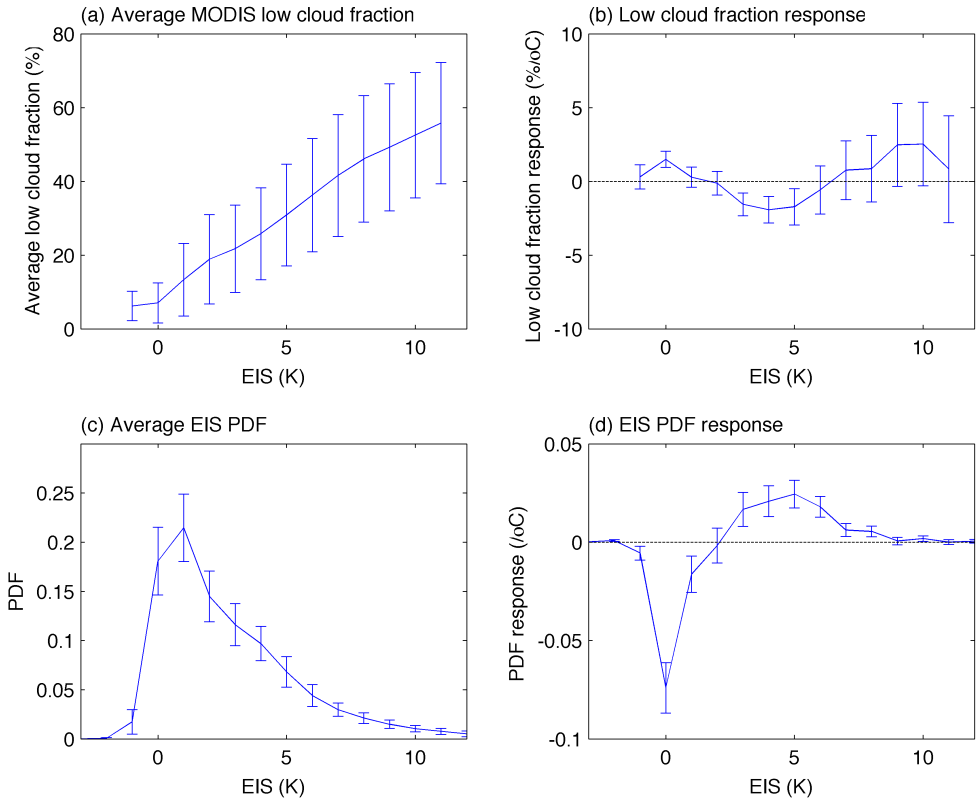

Figure 4.5 Contribution of EIS on low cloud fraction response. (a) Average low cloud fraction as a function of EIS. (b) Low cloud fraction response to inter-annual surface warming as a function of EIS. (c) Probability density function (PDF) of EIS. (d) EIS PDF response to inter-annual surface warming. Error-bars are 1-σ uncertainty intervals, and only tropical clouds over oceans are included.

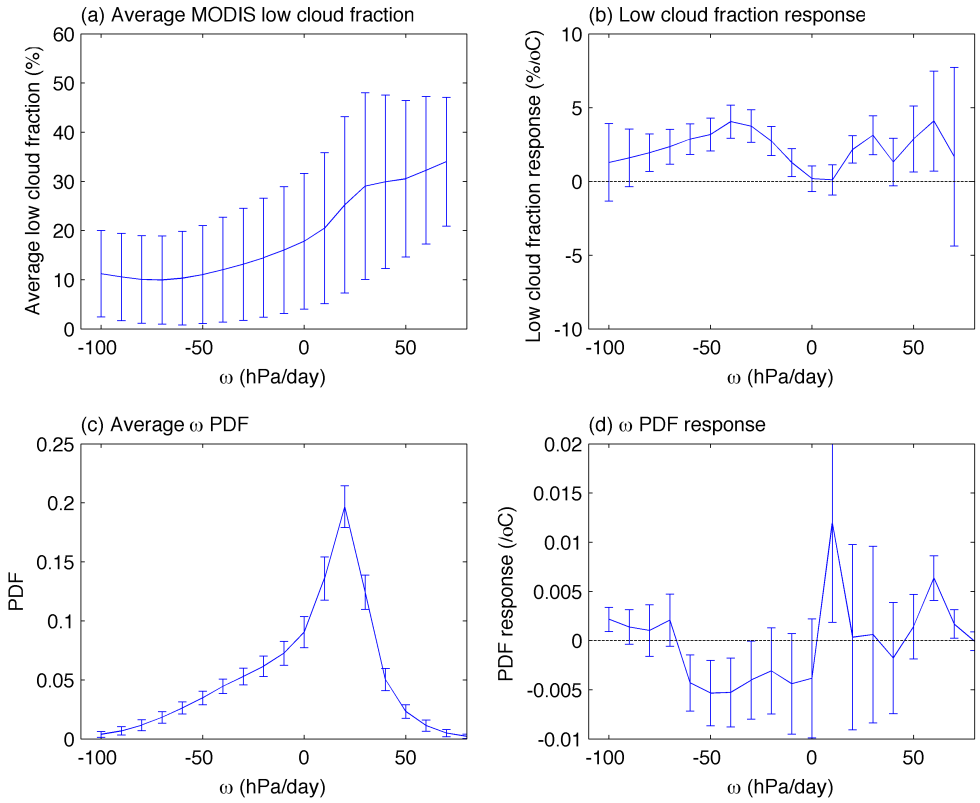

Figure 4.6 Contribution of vertical velocity at 500hPa (ω) on low cloud fraction response. (a) Average low cloud fraction as a function of vertical velocity. (b) Low cloud fraction response to inter-annual surface warming as a function of vertical velocity. (c) PDF of vertical velocity. (d) Vertical velocity PDF response to inter-annual surface warming. Error-bars are 1-σ uncertainty intervals, and only tropical clouds over oceans are included.

Table 4.1 Attribution of short-term low cloud response.

Variable	Value	Note	Effect on low cloud fraction response
$C_{\omega}*dP_{\omega}/dT_s$	0.15	Large-scale dynamic component	Minor
$P_{\omega}*dC_{\omega}/dT_s$	1.93	Thermodynamic component	Major
$C_{EIS}*dP_{EIS}/dT_s$	2.25	EIS	Major
$P_{EIS}*dC_{EIS}/dT_s$	-0.08	Non-EIS component	Minor

We use the method of Bony et al. (2004) to determine whether the positive tropical low cloud response to inter-annual surface warming is induced by responses of EIS. The tropical low cloud fraction can be calculated as

$$C = \sum C_{EIS} P_{EIS} , \tag{4.4}$$

where C_{EIS} is the average low cloud fraction for a given EIS value, P_{EIS} is the probability function. Then we have

$$\frac{dC}{dT_s} = \sum C_{EIS} \frac{dP_{EIS}}{dT_s} + \sum P_{EIS} \frac{dC_{EIS}}{dT_s} , \tag{4.5}$$

the low cloud fraction response is a summation of EIS component (first item on the right side) and non-EIS component (second item on the right side).

Figure 4.5(a) shows the average low cloud fraction as a function of EIS over oceans (C_{EIS}), and the low cloud fraction response to inter-annual surface warming as a function of EIS is shown in Figure 4.5(b). Figure 4.5(c) shows the probability density function (PDF) of EIS, and Figure 4.5(d) is the EIS PDF response to inter-annual surface warming. Then the low cloud response induced by EIS changes is $C_{EIS}*dP_{EIS}/dT_s$, and the low cloud response induced by non-EIS components is $P_{EIS}*dC_{EIS}/dT_s$. The values are listed in Table 4.1, and apparently the tropical low cloud fraction response is primarily induced by changes in EIS over oceans.

Contribution from large-scale dynamics is also studied using Bony's method (Figure 4.6). The large-scale dynamic component has small effect on tropical low cloud response (Table 4.1), which is consistent to Bony et al. (2004).

However, climate models do not show a good relationship between low cloud fraction and EIS (Caldwell et al. 2013). The relationship between tropical EIS and average cloud fraction in the boundary layer (800-100hPa) in GFDL-CM3 is plotted in Figure 4.7. Therefore, it is inferred that the inconsistency of low cloud fraction response in models and observations is primarily induced by the bad EIS-low cloud fraction relationship in climate models. Caldwell et al. (2013) simulated the low cloud using an off-line boundary layer model, and suggested that the low cloud fraction response to global warming is net negative.

4.3 Evaluation of long-term cloud feedback

Cloud feedbacks in response to surface temperature trend and variability are both positive in climate models, but the magnitude of cloud feedback has large spread among models. Uncertainty in PBL clouds in GCMs is the primary source of the large spread in GCM predicted cloud feedbacks. If the PBL cloud response is given, short-term and long-term cloud feedback in response to tropical surface temperature trend and variability are the same in climate models.

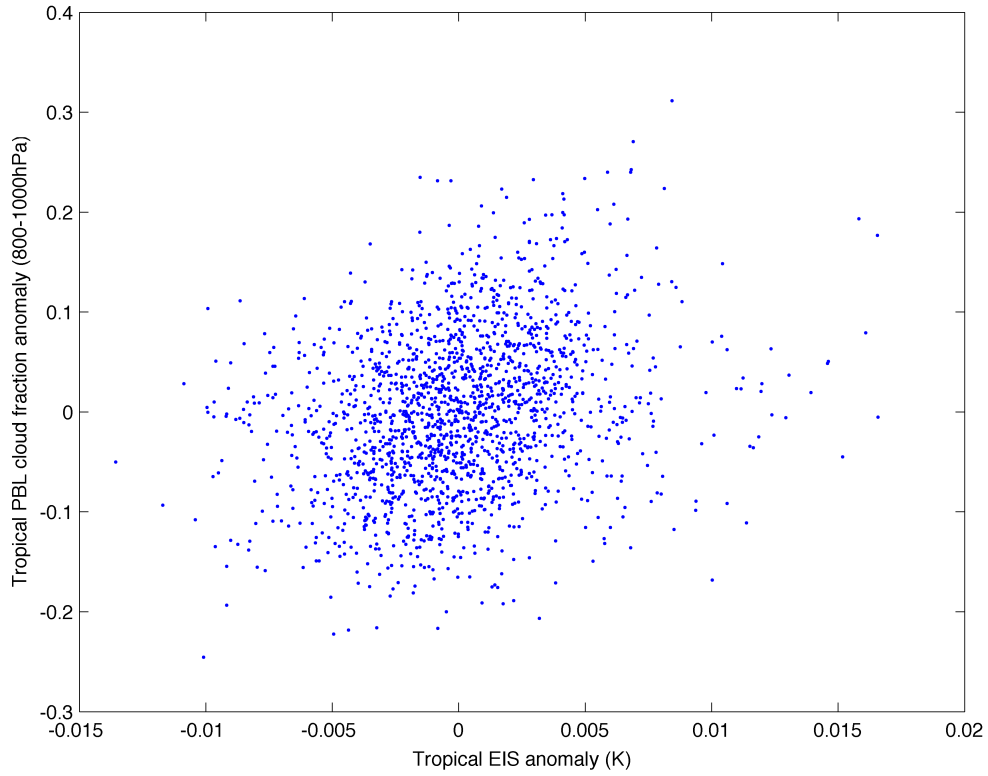

Figure 4.7 Relationship between tropical EIS anomaly and low cloud fraction anomaly in GFDL-CM3 control run.

Observations suggest that the tropical low cloud fraction increases in response to tropical surface temperature variability, but most climate models show a negative response. The disagreement between models and observations is induced by the poor EIS-low cloud fraction relationship in climate models. The positive short-term tropical low cloud fraction response in observations results from changes in EIS, and changes in large-scale dynamics have little impact on the low cloud responses. If the EIS-low cloud fraction relationship holds under global warming, it is likely that the tropical low cloud fraction change is proportional to the change in tropical EIS. Therefore, we discuss mechanisms that may lead to EIS changes.

Change in spatial surface temperature variation may result in EIS change. However, HadISST (Rayner et al., 2003) dataset suggests that the spatial surface temperature variation is close to zero during the last 140 years, so the change of spatial surface temperature variation has small effect on EIS under global warming. Downward heat transport is likely to increase in response to surface warming, because the upper troposphere warms more than the lower troposphere (Figures 3.1-3.3).

Climate models suggest that tropical EIS will increase under global warming (Figure 4.8). EIS over oceans increases more than EIS over land, because the magnitude of sea surface warming is less than land, but the 700hPa temperature change over land and oceans are close due to horizontal winds in the free atmosphere. If the observed EIS-low cloud fraction holds under long-term global warming, it is likely that tropical low cloud change is non-negative under global warming.

Among the fifteen models included in this thesis, six models show a significantly negative tropical low cloud response to long-term global warming, and the other nine models do not. If the tropical low cloud fraction changes are not significantly negative, then results from the latter nine models can be used to estimate the long-term cloud feedback. The estimated long-term cloud feedback is 0-0.5 $W/m^2/°C$, and the ECS is 1.5-3.5 °C.

Our result is opposite to, but does not conflict with Sherwood et al. (2014). Sherwood et al. (2014) found that the spread low cloud feedback in climate models could be explained by the spread in climatological lower-tropospheric mixing index, and the lower-tropospheric mixing index in reanalysis is consistent with climate models that have large climate sensitivity. However, the observed EIS-low cloud relationship is poorly simulated in climate models, so the model predicted relationship between the low cloud feedback and the climatological lower-tropospheric mixing index may have systematic error, thus the climate sensitivity may also be overestimated. On the other hand, the lower-tropospheric mixing index is a summation of two indexes, small-scale mixing index S, and large-scale mixing index D. We found that S (calculated from ERA-interim) is better correlated with the MODIS low cloud fraction, but D is not well correlated with low cloud fraction, indicating that the large-scale mixing does not have significant effect on low cloud fraction. Both observations and climate models suggest S will decrease in response to inter-annual and long-term surface warming, suggesting a negative low cloud feedback, this is consistent with our results.

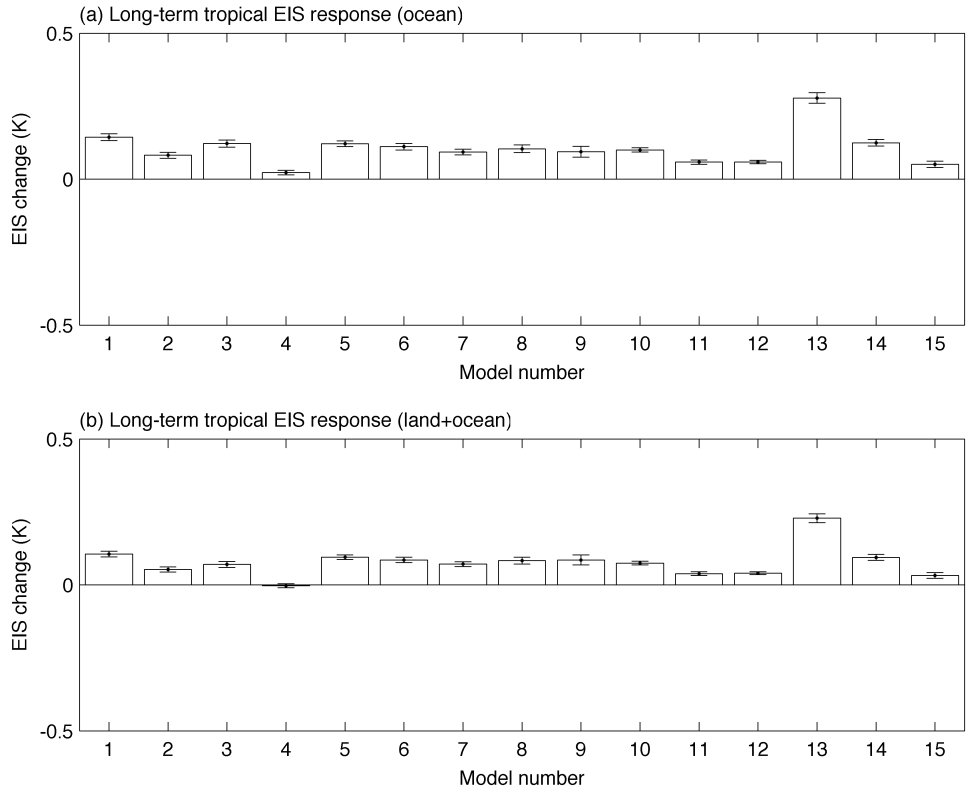

Figure 4.8 Long-term EIS response calculated from CMIP5 4xCO_2 experiments. (a) Ocean only. (b) Land + Ocean. Each bar represent the EIS change in a model, and the model numbers are listed in Table 3.1.

5. CONCLUSIONS

In this thesis, we calculate the short-term cloud feedback with observations, and compared with short-term cloud feedback in climate models. A link between short-term and long-term cloud feedback in climate models is established to evaluate the long-term cloud feedback in climate models.

Observations suggest that there are more low clouds in the planetary boundary-layer in response to inter-annual surface warming, contributing a negative cloud feedback; the overall cloud optical depth decreases, contributing a positive cloud feedback; there is an overall increases in cloud top pressure for clouds in the free atmosphere, contributing a positive feedback. The total cloud feedback in response to global surface warming is likely positive, but with large uncertainty.

Climate models generally show a positive cloud feedback in response to surface temperature trend and variability. In response to surface temperature changes, there is a decrease in the middle/low cloud amount and an increase in high cloud amount, indicating an overall increase in cloud height.

The spatial pattern of short-term cloud response to surface temperature trend is different from the spatial pattern of long-term cloud response to surface temperature variability. However, integrating over the tropics, the vertical profiles of cloud responses to tropical surface temperature trend and variability are the same.

Uncertainty of PBL clouds in GCMs is the primary source of the large spread in GCM predicted cloud feedbacks. Observations suggest that the tropical low cloud

fraction increases in response to inter-annual surface warming, but most climate models show a negative response. The disagreement between models and observations is induced by the poor EIS-low cloud fraction relationship in climate models. The positive short-term tropical low cloud fraction response in observations results from changes in EIS, and changes in large-scale dynamics have little impact on the low cloud responses. Most climate models suggest that EIS will increase under long-term global warming. If the EIS-low cloud fraction relationship holds under global warming, it is likely that the tropical low cloud fraction changes are not negative. Climate models without significant negative low cloud fraction change suggest that the cloud feedback is 0-0.5 $W/m^2/°C$, and the corresponding ECS is 1.5-3.5 °C.

REFERENCES

Allan, R. P., 2011: Combining satellite data and models to estimate cloud radiative effect at the surface and in the atmosphere, Meteorological Applications, 18, 324-333.

Bindoff, N.L., P.A. Stott, K.M. AchutaRao, and et al., 2013: Detection and attribution of climate change: from Global to Regional. In: Climate change 2013: The physical science basis. Contribution of working group I to the fifth assessment report of the intergovernmental panel on climate change. Cambridge University Press, Cambridge, United Kingdom and New York, NY, USA.

Bony, S., J.-L. Dufresne, H. L. Treut, J. J. Morcrette, and C. Senior, 2004: On dynamic and thermodynamic components of cloud changes. Climate Dynamics, 22, 71-86.

Bony, S., and J. L. Dufresne, 2005: Marine boundary layer clouds at the heart of tropical cloud feedback uncertainties in climate models. Geophys. Res. Lett. 32, L20806.

Caldwell, P. M., Y. Zhang and S. A. Klein, 2013: CMIP3 subtropical stratocumulus feedback interpreted through a mixed-layer model. J. Clim., 26, 1607-1625.

Clement, A. C., R. Burgman, and J. R. Norris, 2009: Observational and model evidence for positive low-level cloud feedback, Science, 325, 460-464.

Collins, M., R. Knutti, J. Arblaster, J.-L. Dufresne, and et al., 2013: Long-term climate change: Projections, commitments and irreversibility. In: Climate change 2013: The physical science basis. Contribution of working group I to the fifth assessment report of the intergovernmental panel on climate change. Cambridge University Press, Cambridge, United Kingdom and New York, NY, USA.

Colman, R. A., 2003: A comparison of climate feedbacks in general circulation models, Climate Dynamics, 20, 865-873.

Cubasch, U., D. Wuebbles, D. Chen, M.C. Facchini, D. Frame, N. Mahowald, and J.-G. Winther, 2013: Introduction. In: Climate change 2013: The physical science basis. Contribution of working group I to the fifth assessment report of the intergovernmental panel on climate change. Cambridge University Press, Cambridge, United Kingdom and New York, NY, USA.

Dee, D. P., S. M. Uppala, A. J. Simmons, and et al., 2011: The ERA-Interim reanalysis: Configuration and performance of the data assimilation system, Q. J. R. Meteor. Soc., 137, doi:10.1002/qj.828, 553-597.

Dessler, A. E., and P. Yang, 2003: The distribution of tropical thin cirrus clouds inferred from Terra MODIS data, J. Climate, 16, 1241-1248.

Dessler, A. E., 2010: A determination of the cloud feedback from climate variations over the past decade, Science, 330, doi:10.1126/science.1192546, 1523-1527.

Dessler, A.E., 2013: Observations of climate feedbacks over 2000-2010 and comparisons to climate models, J. Climate, 26, 333-342, doi: 10.1175/JCLI-D-11-00640.1.

Donovan, D. P., 2003: Ice-cloud effective particle size parameterization based on combined lidar, radar reflectivity, and mean Doppler velocity measurements. J. Geophys. Res. 108, D18, 2156-2202.

Evan, A. T., A. K. Heidinger, and D. J. Vimont, 2007: Arguments against a physical long-term trend in global ISCCP cloud amounts, Geophys. Res. Lett., 34, L04701, doi:10.1029/2006GL028083.

Fu, Q. and K. N. Liou, 1992: On the correlated k-distribution method for radiative transfer in nonhomogeneous atmospheres. J. Atmos. Sci. 49, 2139-2156.

Fueglistaler, S., et al., 2009: The tropical tropopause layer. Rev. Geophys. 47, RG1004.

Hansen, J., R. Ruedy, M. Sato, and K. Lo, 2010: Global surface temperature change, Rev. Geophys., 48, Rg4004, doi:10.1029/2010rg000345.

Hartmann, D. L., and Larson, 2002: K. An important constraint on tropical cloud-climate feedback. Geophys. Res. Lett., 29.

Holton, J. R., 1994: An introduction to dynamic meteorology. Academic Press, New York.

Houghton, J. T., Ding, Y., Griggs, D. J., Noguer, M., Van der Linden, P. J., Dai, X., Maskell, K. and Johnson, C. A. (Eds.), 2001: IPCC Climate change 2001: The scientific basis. Contribution of working group I to the third assessment report of the intergovernmental panel on climate change. Cambridge University Press, Cambridge and New York.

Hu, Y. and Fu, Q.: Observed poleward expansion of the Hadley circulation since 1979, Atmos. Chem. Phys., 7, 5229-5236, doi:10.5194/acp-7-5229-2007, 2007.

Hu, Y., C. Zhou, and J. Liu, 2011: Observational evidence for poleward expansion of the Hadley Circulation. Adv. Atmos. Sci., 28, 33-44.

Hubanks, P. A., M. D. King, S. Platnick, and R. Pincus, 2008: MODIS Atmosphere L3 gridded product algorithm theoretical basis document, Rep. ATBD-MOD-30.

Josset, D., J. Pelon, A. Garnier, and et al., 2012: Cirrus optical depth and lidar ratio retrieval from combined CALIPSO-CloudSat observations using ocean surface echo, J. Geophys. Res., 117, D05207, doi:10.1029/2011JD016959.

King, M. D., Y. J. Kaufman, W. P. Menzel, and D. Tanre, 1992: Remote sensing of cloud, aerosol, and water vapor properties from the Moderate Resolution Imaging Spectrometer (MODIS), Ieee Trans. Geosci. Remote, 30, 2-27.

Liou, K. N., 1986: Influence of cirrus clouds on weather and climate Processes: A global perspective. Monthly Weather Review 114 (6), 1167.

Liou, K. N., 2005: Cirrus clouds and climate. McGraw-Hill 2005 Yearbook of Science & Technology 51–53 (McGraw-Hill).

Loeb, N. G., S. Kato, W. Su, T. Wong, F. Rose, D. R. Doelling, J. R. Norris, and X. Huang, 2012: Advances in understanding top-of-atmosphere radiation variability from satellite observations, Surveys in Geophysics, 33, doi:10.1007/s10712-012-9175-1, 359-385.

Lu, J., Chen, G. and D.M.W. Frierson, 2008. Response of the zonal mean atmospheric circulation of El Nino versus global warming. J. Climate, 21: 5835-5851.

Lynch, D. K., 1996: Cirrus clouds: Their role in climate and global change. Acta Astronautica 38 (11), 859-863.

Marchand, R., T. Ackerman, M. Smyth, and W. B. Rossow, 2010: A review of cloud top height and optical depth histograms from MISR, ISCCP, and MODIS, J. Geophys. Res., 115, D16206, doi:10.1029/2009jd013422.

Morice, C. P., J. J. Kennedy, N. A. Rayner, and P. D. Jones, 2012: Quantifying uncertainties in global and regional temperature change using an ensemble of observational estimates: The HadCRUT4 data set, J. Geophys. Res., 117, D08101, doi:10.1029/2011jd017187.

Pincus, R., S. Platnick, S. A. Ackerman, R. S. Hemler, and R. J. P. Hofmann, 2012: Reconciling simulated and observed views of clouds: MODIS, ISCCP, and the limits of instrument simulators. J. Climate 25, 4699-4720.

Platnick, S., M. D. King, A. S. Ackerman, W. P. Menzel, B. A. Baum, J. C. Riedi, and R. A. Frey, 2003: The MODIS cloud products: Algorithms and examples from Terra, Ieee Trans. Geosci. Remote, 41, 459-473.

Qu, X., A. Hall, and S. A. Klein, and P. M. Caldwell, 2013: On the spread of changes in marine low cloud cover in climate model simulations of the 21st century. Clim. Dyn. , doi:10.1007/s00382-013-1945-z.

Randall, D. A., et al., 2007: Climate models and their evaluation. In: Climate change 2007: The physical science basis. Contribution of working group I to the fourth assessment report of the intergovernmental panel on climate change. Cambridge University Press, Cambridge, United Kingdom and New York, NY, USA, pp. 589–662.

Rayner, N. A., D. E. Parker, E. B. Horton, and et al., 2003: Global analyses of sea surface temperature, sea ice, and night marine air temperature since the late nineteenth century, J. Geophys. Res., Vol. 108, No. D14, 4407.

Rienecker, M. M., et al., 2011: MERRA - NASA's modern-era retrospective analysis for research and applications, J. Climate, 24, doi:10.1175/JCLI-D-11-00015.1, 3624-3648.

Rosenzweig, C., G. Casassa, D.J. Karoly, and et al., 2007: Assessment of observed changes and responses in natural and managed systems. Climate change 2007: impacts, adaptation and vulnerability. Contribution of working group II to the fourth assessment report of the intergovernmental panel on climate change, Cambridge University Press, Cambridge, UK, 79-131.

Schneider, S.H., S. Semenov, A. Patwardhan, and et al., 2007: Assessing key vulnerabilities and the risk from climate change. Climate change 2007: Impacts, adaptation and vulnerability. Contribution of working group II to the fourth assessment report of the intergovernmental panel on climate change. Cambridge University Press, Cambridge, UK, 779-810.

Sherwood, S. C., S. Bony, and J. L. Dufresne, 2014: Spread in model climate sensitivity traced to atmospheric convective mixing, Nature 505, 37–42.

Shell, K. M., J. T. Kiehl, and C. A. Shields, 2008: Using the radiative kernel technique to calculate climate feedbacks in NCAR's Community Atmospheric Model, J. Climate, 21, doi:10.1175/2007jcli2044.1, 2269-2282.

Smith, T. M., R. W. Reynolds, T. C. Peterson, and J. Lawrimore, 2008: Improvements to NOAA's historical merged land-ocean surface temperature analysis (1880-2006), J. Climate, 21, doi:10.1175/2007jcli2100.1, 2283-2296.

Soden, B. J., and I. M. Held, 2006: An assessment of climate feedbacks in coupled ocean-atmosphere models, J. Climate, 19, 3354-3360.

Soden, B. J., I. M. Held, R. Colman, K. M. Shell, J. T. Kiehl, and C. A. Shields, 2008: Quantifying climate feedbacks using radiative kernels, J. Climate, 21, 3504-3520.

Taylor, K. E., R. J. Stouffer, and G. A. Meehl, 2012: An overview of CMIP5 and the experiment design. Bull. Amer. Meteor. Soc. 93, 485–498.

Trenberth, K. E., and J. W. Hurrell, 1994: Decadal atmosphere-ocean variations in the Pacific, Climate Dynamics, 9, doi:10.1007/bf00204745, 303-319.

Vial, J., J. L. Dufresne, and S. Bony, 2013: On the interpretation of inter-model spread in CMIP5 climate sensitivity estimates. Clim. Dyn., 41: 3339-3362.

Wood, R., and C. S. Bretherton, 2006: On the relationship between stratiform low cloud cover and lower-tropospheric stability. J. Climate, 19, 6425–6432.

Winker, D. M., J. R. Pelon, and M. P. McCormick, 2003: The CALIPSO mission: spaceborne lidar for observation of aerosols and clouds, Proc. SPIE 4893. Lidar Remote Sensing for Industry and Environment Monitoring III 1-11.

Zelinka, M. D., and D. L. Hartmann, 2011: The observed sensitivity of high clouds to mean surface temperature anomalies in the tropics, J. Geophys. Res., 116, D23103, doi:10.1029/2011jd016459.

Zelinka, M. D., S. A. Klein, and D. L. Hartmann, 2012a: Computing and partitioning cloud feedbacks using cloud property histograms. Part I: Cloud radiative kernels, J. Climate, 25, doi:10.1175/jcli-d-11-00248.1, 3715-3735.

Zelinka, M. D., S. A. Klein, and D. L. Hartmann, 2012b: Computing and partitioning cloud feedbacks using cloud property histograms. Part II: Attribution to changes in cloud amount, altitude, and optical depth, J. Climate, 25, doi:10.1175/jcli-d-11-00249.1, 3736-3754.

Zelinka, M. D., S. A. Klein, K. E. Taylor, T. Andrews, M. J. Webb, J. M. Gregory, and P. M. Forster, 2013: Contributions of different cloud types to feedbacks and rapid adjustments in CMIP5. Journal of Climate, 26, 5007-5027.

Zhang, Y., S. Xie, C. Covey, D. D. Lucas, P. Gleckler, S. A. Klein, J. Tannahill, C. Doutriaux, and R. Klein, 2012: Regional assessment of the parameter-dependent performance of CAM4 in simulating tropical clouds, Geophys. Res. Lett., 39, L14708, doi:10.1029/2012GL052184.

Zhou, C., P. Yang, A. E. Dessler, Y.-X. Hu, and B .A. Baum, 2012: Study of horizontally oriented ice crystals with CALIPSO observations and comparison with Monte Carlo radiative transfer simulations, J. Appl. Meteor. Climatol., 51, 1426–1439. doi: 10.1175/JAMC-D-11-0265.1.

Zhou, C., P. Yang, A. E. Dessler, and F. Liang, 2013: Statistical properties of horizontally oriented plates in optically thick clouds from satellite observations. IEEE Geosci. Remote Sens. Lett., 10, 986-990, doi:10.1109/LGRS.2012.2227451.

Zhou, C., M.D. Zelinka, A.E. Dessler, P. Yang, 2013: An analysis of the short-term cloud feedback using MODIS data, J. Climate, 26, 4803-4815, doi:10.1175/JCLI-D-12-00547.1.